ABSTRACT

Title of Thesis:	QUANTIFYING ERRORS IN LARGE SCALE WATER BALANCE
	Sommer Nicole Joe, Master of Science, 2004
Thesis Directed By:	Dr. Kaye L. Brubaker, Department of Civil and Environmental Engineering

Assessment and prediction of the effects of Arctic river flows on ocean circulation and climate are hindered by lack of knowledge about the terrestrial water balance. This study quantifies the components of the annual water budget (precipitation, streamflow, and evapotranspiration) and their uncertainty for a large Russian river basin. Over long periods, assuming negligible change in storage, inputs and outputs should balance. However, measurement limitations and errors lead to nonzero water balance closure (WBC). The variance of WBC, computed by summing the component variances, quantifies uncertainty in the water budget. The component terms and their uncertainty are calculated from independent observations and physically-based modeling. For the analysis period, the WBC is negative. The computed uncertainty is large, but not sufficient to conclude that WBC could be zero. Because current assessments do not completely account for the water budget, statements about the effects of climate change must be done cautiously.

QUANTIFYING ERRORS IN LARGE SCALE WATER BALANCE

By

Sommer Nicole Joe

Thesis submitted to the Faculty of the Graduate School of the
University of Maryland, College Park, in partial fulfillment
of the requirements for the degree of
Master of Science]
2004

Advisory Committee:
Dr. Kaye L. Brubaker Chair
Dr. Richard McCuen
Dr. Glenn Moglen

Table of Contents

List of Figures

List of Tables

1 Introduction

1.1 Context of Research

This thesis is part of a larger study to quantify the freshwater fluxes of the Ob River basin in Russian Siberia. The larger study is a joint research effort with Micheal Jasinski and Jeremy Stoll (NASA group), scientist and researchers at the National Aeronautic Space Administration at Goddard Space Flight Center. The study is looking at the effect the snowpack in the Eurasian mountains and Siberian plain has on the fresh water fluxes and the Arctic water cycle. The goal is to use remote sensing and hydrological modeling to improve the understanding of the contribution of snowpack processes to the water budget of the Ob river basin. It will also look at how the freshwater discharge from the Ob River affects the Arctic water cycle. The larger study will serve as an important indication of the climate sensitivity and controls of freshwater fluxes in the Artic Ocean (Brubaker et al. 2000).

The amount and timing of freshwater supply to the Artic Ocean are currently a topic of great interest to studies of the world oceans and global climate. Though the Artic Ocean only holds 1.5% of the world's total water volume, it drains 10% of the world's total surface runoff (ACSYS, 1992). The freshwater fluxes discharging into the ocean are said to be the driving cause in the global climate change (Gagosian, 2003). The freshwater discharge into the ocean causes a change in the vertical stability of the ocean. The basic circulation pattern in the arctic water is that cold water sinks, bringing warmer water to the top. The freshwater discharge into the ocean makes the water less dense and this could have two possible effects. The dilution of the waters could cause the sinking of the cold water to stop since the heavy salty water usually sinks, which creates an in-

ocean circulation pattern. The fresh water could also cause an insulating layer, thus cooling the ocean waters by suppressing heat exchange with the atmosphere. These effects could cause a change in the ocean current patterns which in turn could cause a change in the global climate since ocean currents affect air temperature and therefore air circulation around the globe.

The Ob River is a major contributor to the Artic Ocean. The Ob has the third greatest discharge of Siberia's rivers; on average, it pours 95 cubic miles (400 cubic km) of water annually into the Arctic Ocean—about 12 percent of the ocean's total intake from drainage (Britannica, 1994). The basin of the Ob River covers an area of 2,700,000 km^2 and is located in Russia in the Siberian region; it is the fourth largest basin in the world in terms of drainage area (Dingman, 2002). The Ob River begins in the Altai Mountains, flows north, and drains to the Arctic Ocean.

Like other Arctic rivers, the Ob experiences springtime flooding due to snowmelt and ice jams. Springtime snowmelt flooding is a major problem in the Siberian region. The region suffers long, harsh winters, and short mild summers. Heavy snow falls in the mountain regions. Snow in the mountain regions averages 80 inches annually and the forested region range from 24-36 inches annually. Snow cover usually lasts for approximately 200 days. Springtime flooding in the upper Ob basin begins in April. This is when the snow on the plains begins to melt, but then the area goes through a second phase when the mountain snow begins to melt. Springtime flooding from snowmelt ends in July, but the water level rises again with rain in September and October. The flooding in the upper Ob obstructs the drainage of the rivers' tributaries such as the Tom River basin (Brittanica, 1994). In addition to snowmelt flooding, ice

jams on the river cause flooding also. The entire river is frozen by the end of November and stays frozen for about 150-220 days depending on location. The thawing takes about a month, from the end of April to the end of May. The ice jams cause flooding by obstructing the flow of water. The flow either builds up causing overflow of the banks of the river or, once the ice block is melted or eroded away, the backed up water flows causing a higher than usual amount leading to flooding. This is a problem for the Ob as well as many of its tributaries with mountain origins.

In order to predict the potential consequences of large scale climate change (such as expected global warming), it is essential to quantify and understand the supply and storage of fresh water in Arctic basins such as the Ob. In order to accurately assess the effects of freshwater discharge into the ocean it is necessary to quantify the potential amount of discharge, hence the supply and storage of water in the basins. The freshwater in Arctic basins, such as the Ob, discharges about 35 cm per year into the Arctic Ocean, making rivers the primary source of freshwater to the ocean (Serreze et al., 2003). For the Ob River, the main source of water for the river is seasonal snowmelt and rainfall (Brittanica, 1994). If the snow and other forms of precipitation in the mountains are not accurately accounted for, the snowmelt cannot be accurately quantified, thus leading to an inaccurate estimate of the amount of freshwater discharge into the Arctic Ocean. The supply and storage of freshwater in the basin is needed in order to quantify the freshwater fluxes into the ocean.

It is equally important to quantify the level of uncertainty in statements about the components of the Artic water balance. The uncertainty in the components is an indication of the accuracy of estimates of the components and the confidence in the

estimates. The confidence in the components and the water balance can be used to determine the limitations of the use in such cases as predicting the effect of climate changes.

1.2 Problem Statement

This thesis addresses the question, "How confident can we be in current estimates of fresh water budget components for the Ob River?" The current estimates of precipitation are not very accurate because the river basin is sparsely gaged due to its terrain. The mountainous regions make it hard to position and maintain gages, yet the precipitation in the mountains has larger yearly amounts than the other regions in the watershed due to the snow. This under representation of gages leads to precipitation being annually underestimated, possibly by as much as 50% (Brubaker et al., 2000). Also sampling variability is an issue. The gage network can't accurately capture the entire amount of precipitation that falls in the mountainous regions due to terrain variability and the costly factor of installing numerous gages in the mountains. It is more costly to install and maintain a gage in the mountain than in flat, easily reachable land. The misrepresentation of precipitation in the water balance leads to error in any water budget quantities derived from precipitation. Precipitation is the basic input into the water balance for a region; if the input is not accurately quantified than the outputs will also be in error.

Assuming negligible change in storage over a 1-yr time period, the water budget of a region should be in balance. The simplified theoretical water balance for a region is,

$$P - Q - E = 0 \tag{1-1}$$

where P is precipitation, Q is streamflow, and E is evapo(transpi)ration. The equation is simplified to the basic inputs and outputs into the system. Since the change in storage is

being ignored, the region is assumed to be a conservative system, thus the inputs should

equal the outputs.

Errors in measuring or estimating the terms in equation 1-1 lead to a non-zero

total, or water balance closure (WBC):

$$WBC = P - Q - E \tag{1-2}$$

Hydrologists and water resources managers share the goal of balancing the water budget

by trying to determine the sources of error leading to a nonzero water balance closure.

However, before trying to fix the budget imbalance, it is useful to determine how

significantly different from zero the water balance closure really is. This can be

determined by estimating a confidence interval (or an error bar) on the water balance

closure.

Uncertainty in the water balance can be quantified by the variance in the water

balance closure. The error in each component can be quantified as the variance of the

basin average estimates. The error in the water balance closure is propagated through the

variance of the estimates of each term. Assuming that the errors of each term are

independent of each other, the variance of the water balance closure is the sum of the

term variances (Dingman, 1994):

$$S^2(WBC) = S^2(P) + S^2(Q) + S^2(E) \tag{1-3}$$

where S^2 is the variance of the term. The variance of the water balance closure can be

used to construct a confidence interval for the water balance closure at a chosen level of

confidence.

1.3 Research Goals and Objectives

The goal of this research is to determine the variance of the water balance closure by calculating the individual variance of the components and to assess the accuracy of the water balance through its bias and precision. To accomplish this goal, the objectives of this research are:

1) Calculate the areal average of precipitation, streamflow, and evapotranspiration for the Tom River basin using available measurements for five water years (1981-1985) through independent calculations using a variety of measurements characterized by different levels of uncertainty.

2) Quantify the uncertainty in each basin-average term for each water year. Different methods for each term in the water balance will be used to perform this task.

3) Calculate the water balance closure (equation 1-1) for each water year.

4) Calculate the variance of the water balance closure (equation 1-2) for each water year.

5) Construct confidence intervals on the water balance closure for each water year.

6) Perform statistical hypothesis tests on whether the water balance closure is non-zero.

This study is limited to the Tom River basin for the years 1980 through 1985. The Tom River basin is a sub basin of the Ob river basin. The upper Ob River basin begins where the Tom River discharges into the Ob River at the city of Tomsk (**Figure 1.1**).

Figure 1.1 Map of Siberia, Russia. Includes Tom River and location of outlet to Ob River at Tomsk.

The Tom River, which is the location of important cities in the Siberian region, has readily available data due to its importance in the region. Though much smaller than the Ob River in flow and drainage area, the Tom River basin is an important factor in determining the conditions of the Ob River basin.

This thesis will contribute to the goals of a larger study. The NASA group decided that the Tom basin would be suitable to develop methods for this study, then apply them to the larger Ob basin. This work can then be applied to other basins around the world with similar conditions.

1.4 Justification of Expected Results

Based on our previous knowledge about the basin the following results are expected:

1) The water balance closure is expected to be biased low (WBC < 0) due to underestimation of precipitation (P) in the mountains.

2) Due to the level of uncertainty in the water balance components, the water balance closure will not be significantly different from zero for typical confidence levels (90% and greater).

3) Different terms in the water balance will contribute different degrees of uncertainty to the water balance closure.

If these results are in fact true, these still leave the question of how to lessen the amount of uncertainty in the water balance and how this uncertainty affects its practical use.

2 Literature Review

2.1 *Introduction to Large Scale Water Balance*

The water balance of a watershed follows the conservation of mass principle. The water
that enters a defined region (such as a watershed) through precipitation and groundwater
less that which exits through evapotranspiration, streamflow, and groundwater flow must
equal the change in storage in the region,

$$\Delta S = P + G_{in} + Q_{in} - Q_{out} - E - G_{out} \qquad (2\text{-}1)$$

where ΔS is the change in storage, P is precipitation, Q_{in} is surface flows into the region
including artificial transfers, Q_{out} is streamflow, E is evapotranspiration, and G_{in} and G_{out}
are groundwater flow to and from the region, respectively. The equation is evaluated
over some specified period of time; each of its terms has units of mass, volume, or depth
(volume divided by the region's area). When looking at the water balance for a
watershed on a long term basis, several terms in Equation (2-1) can be neglected
(Dingman 2002). Surface flows into a region (Q_{in}) can be considered zero for a
watershed without artificial inflows. Groundwater inflow is neglected due to the
assumption that the surface boundaries of the watershed also constitute groundwater
boundaries. Groundwater flow out of the watershed is usually small because
groundwater makes its way to the stream network as baseflow and appears as surface
discharge, Q.

An argument can be made that if long-term averages of the inflow and outflows
are made, then the change in storage is approximately zero because physically an average
positive change in storage (gain in moisture) or negative change in storage (loss) cannot
be sustained over the long term. The change in storage can also be assumed small if the

water balance is analyzed over an annual cycle such as the water year. The water year is different from the calendar year; the water year begins October 1 and ends September 30 in the northern hemisphere since the annual flow cycle and storage of water in soil, vegetation, and water bodies is usually its lowest around this time.

With groundwater flow, surface inflows, and change in storage being negligible, this leaves the three main physical processes of the water balance on a long term or water year basis to be precipitation, streamflow, and evapotranspiration,

$$\overline{P} - \overline{Q} - \overline{E} = 0 \tag{2-2}$$

where the overbar notation indicates long-term average of the respective quantities.

Either equation 2-1 or 2-2 can be used to estimate terms of the water balance as residuals. This method is usually used for terms that are hard to measure such as vertical leakage, groundwater flow, and E. When the other values are known, the term being calculated as a residual is simply obtained through subtraction. The use of a lysimeter to estimate evapotranspiration incorporates this idea. The lysimeter is a block of soil buried in the ground; the inflows and outflows are measured for the block of soil over a period of time. The drainage type of lysimeter doesn't account for changes in storage, thus is only useful when the change in storage is negligible; whereas the weighing type does measure changes in storage. Evapotranspiration is calculated as the residual of the water balance for the block of soil.

When calculating a term as a residual of the water balance one has to be careful because the residual contains the net error of all the measured components. It is recommended that all terms being calculated as a residual are labeled and an error analysis is performed (Kondolf et al., 1991).

2.2 Sources & Types of Uncertainty in Each Term

Equation 2-2 is simple, but accurately quantifying each process is difficult. The terms in equation 2-2 typically do not sum to zero, giving rise to a water balance closure. The water balance closure is a result of the individual errors in quantifying each of the three processes. The sources and possible different types of error in each component are discussed below.

The type of uncertainty or error in a measured or estimated quantity is defined by its source. Three types of uncertainty are likelihood, ambiguity, and approximations. We encounter uncertainty due to the natural variability in the quantity being measured and our inability to accurately measure the quantity. The natural variability of the variable can be described in two parts, physical randomness and sampling. Likelihood can be defined in the context of chance, odds, and gambling (McCuen, 2003). Sampling is a source of likelihood uncertainty. Sampling variation causes uncertainty because a sample is used to describe a population, but a sample can rarely accurately quantify the whole population. Ambiguity comes from having multiple possibilities of outcomes for a system, thus recognizing those different possibilities creates the uncertainty (McCuen, 2003). The three main sources of uncertainty in ambiguity are spatial variability, uncertainty in input parameters, and model uncertainty. Physical randomness is a source of ambiguity, where the variable varies in nature, which makes it hard to accurately quantify. Uncertainty from approximations comes from not clearly defining information when developing knowledge. Sources of approximation uncertainty include such things as vagueness in defining parameters, human factors, and defining interrelationships among variables. Our inability to accurately quantify the variable can be described as

11

approximation uncertainty. Human factors cause uncertainty in measurement. There is error in measuring instruments and human error in taking measurements.

Each individual measurement contains a type of error previously discussed. We seek to quantify the cumulative error of the measurements and yield the total error in each term.

Each estimate of any one of the three parameters in equation 2-2 has its own sampling distribution, with a mean and variance. The value provided is the mean or central tendency of the variable, whereas the variance describes the dispersion about the mean. The standard error of an estimate (such as the mean) is the square root of the variance of its sampling distribution. The ambiguity uncertainty is quantified through error bars for the value of the variable. The error bar describes the possible range of values for the variable about the mean value.

2.2.1 Precipitation

Precipitation data contains errors due to measurement accuracy (approximation uncertainty) and the spatial variability (ambiguity & likelihood uncertainty) of precipitation. Milly (2002) described precipitation errors in three parts: orographic effects, gage measurement error, and spatial sampling error. Gage and sampling error are described as random error, and orographic effects are systematic errors, so they can be modeled and removed from the data. Uncertainty from spatial variability is due to the inability of a gage network to accurately sample the study area. Measurement errors are due to the accuracy of the gages. There are two types of precipitation gages, non-recording and recording. Non-recording gages are cylinders open to the air that are emptied at regular intervals to measure the volume of precipitation. Recording gages

measure the volume of precipitation and the timing. Errors from these gages include observer error, location of gage with respect to obstructions, wind effects, evaporation of collected water, horizontal interception, and sensitivity of gage to trace amounts (Dingman, 1988; Dingman 2002). Typically error in snow measurements is much greater than rain measurements mainly due to undercatch (Maidment, 1993). The errors in the individual measurement accumulate when using these point measurements to estimate areal average precipitation in watersheds.

Methods of estimating areal averages of precipitation can be classified into two categories, deterministic and stochastic. Deterministic methods use mathematical formulas to form weighted averages of measured precipitation. The deterministic methods have different methods of assigning weights to each of the gages, and the sum of the weights must equal one. Stochastic methods use weighted averages and statistics that minimize estimation errors to estimate areal distribution of precipitation.

Three common deterministic methods are the station average, Theissen polygon method, and the isohyetal method. The station average assumes equal weight for all gages within the watershed and is simply the mean precipitation of all the gages. That method is ideal for areas of little to no orographic effects, where precipitation gradients across region are not strong, and the spatial distribution of the rain gages is fairly uniform (Dunne, et al., 1998). The Theissen polygon method divides the region into subregions, dictating that all points within the subregion have to be closer to the gage at the center of the subregion than any other gage. The weights are the fraction of the total area occupied by the subregion. The isohyetal method draws isohyets (lines of equal precipitation) for the region. The average precipitation for the area enclosed by adjacent isohyets is the

13

average of the isohyets' value. The weights become the proportion of the total area

enclosed between adjacent isohyets. The Theissen polygon and isohyetal methods both

account for non-uniform spatial distribution of gages and strong precipitation gradients;

however the isohyetal method considers strong gradients caused by topography.

A popular stochastic method is Kriging, which is an interpolation method used to

estimate values at ungaged locations based on existing values at gaged locations using

knowledge about the spatial correlation of a variable. Kriging has been used in numerous

applications such as mapping soil properties, metal concentrations, areal distribution of

temperature, and hydrologic processes: streamflow, and precipitation. It is an attractive

method because not only does it give precipitation estimates at ungaged sites, but it also

gives the error in the estimates. Dingman (1988) and Tsintikidis (2002) both used

kriging to estimate mean annual precipitation and the uncertainties associated with those

values.

2.2.2 Evapotranspiration

Evapotranspiration (E) is often the most uncertain variable due to the fact that it is

the hardest process to measure. Researchers choose to model evapotranspiration or use

real evaporation data obtained from pan methods.

Pan methods use pans placed at ground level, sunk slightly below ground, or

floating on water surfaces, together with an anemometer to measure wind speed and

floating thermometers to measure surface temperature. Evaporation is calculated as the

difference in incoming precipitation and the change in storage of water inside the pan.

Pan evaporation is corrected for wind speed and temperature effects and a pan

14

coefficient, which accounts for energy differences between the pan and a large body such as a lake. This method contains measurement error in resulting evaporation values due to the imperfections in the equipment and human error (approximation uncertainty) and it does not account for evapotranspiration by vegetation.

Modeled evaporation estimates contain error from the model itself and uncertainty in the inputs (ambiguity uncertainty and approximation), although they may be more reliable than field methods because they account for more weather conditions, and the input data required are easier to obtain than field measurements of evaporation. Winter (1981) found that the energy method and mass transfer method were the most reliable method for estimating evaporation compared to field measurements for the regions studied; with error estimates less than 10% and 15%, respectively. Penman (1948) developed a combination equation of the energy budget and mass transfer to estimate evaporation from a free water surface.

Plant transpiration is difficult to accurately measure because of its biological nature. The Penman equation and variations of it are popular methods used to estimate evapotranspiration [Ahn (1996), Moges (2003), and Hupet (2001)].   Monteith introduced vegetation as a source of evapotranspiration, and developed the Penman-Montieth equation, which is generally considered the most realistic model for estimating instantaneous evapotranspiration rates from vegetated areas.

$$ET = \frac{\Delta \cdot (K+L) + \boldsymbol{r}_a \cdot c_a \cdot C_{at} \cdot e_a^* \cdot (1-W_{a)}}{\boldsymbol{r}_w \cdot \boldsymbol{l}_v \cdot \left[\Delta + \boldsymbol{g}\left(1 + \frac{C_{at}}{C_{can}}\right)\right]} \qquad (2\text{-}3)$$

Where Δ (kPa/K) is the rate of change of saturation vapor pressure with respect to temperature, K (MJ/m^2/s) is the net shortwave radiation, L (MJ/m^2/s) is the net longwave radiation, ρ_a (kg/m^3) is the density of air, c_a (MJ/kg/K) is the heat capacity of air, C_{at} [L/T] is the atmospheric conductance, e_a^* (kPa) is the saturated vapor pressure corresponding to air temperature, W_a is the relative humidity, ρ_w (kg/m^3) is the density of water, λ_v (MJ/kg) is the latent heat of vaporization, γ (kPa/K) is the psychometric constant, and C_{can} [L/T] is the canopy conductance. The resultant ET has units of [L/T]. Canopy conductance represents the capacity of the plants to transfer water from the root zone (soil) to the leaf surface (atmosphere). It is dependant on both properties of the plants and the state of the atmosphere. Dingman (2002) suggests the following formulas to calculate canopy conductance:

$$C_{can} = f_s \cdot LAI \cdot C_{leaf} \tag{2-4}$$

$$C_{leaf} = c_{leaf}^* \cdot f_k(K_{in}) \cdot f_r(\Delta r_n) \cdot f_T(T_a) \cdot f_q(\Delta q) \tag{2-5}$$

$$f_k(K_{in}) = \frac{12.78 \cdot K_{in}}{11.57 \cdot K_{in} + 104.4} \tag{2-6}$$

$$f_r(\Delta r_v) = 1 - 66.6 \cdot \Delta r_v \tag{2-7}$$

$$\Delta r_v = \frac{\Delta e \cdot 2.17}{T_a} \tag{2-8}$$

$$f_T(T_a) = \frac{T_a \cdot (40 - T_a)^{1.18}}{691} \tag{2-9}$$

$$f_q(\Delta q) = 1 - 0.00119 \cdot e^{0.81 \cdot \Delta q} \tag{2-10}$$

where f_s is shelter factor, LAI is the leaf area index, c^*_{leaf} [L/T] is the maximum value of leaf conductance (dependent upon vegetation species), K_{in} is incoming shortwave radiation, $\Delta\rho_v$ is the humidity deficit, T_a is the air temperature, and $\Delta\theta$ is the soil moisture deficit. The leaf conductance is function of stomata openings per unit area of the leaf. Stomata opening is affected by five processes: light intensity, CO_2 concentration, vapor pressure deficit, leaf temperature, and leaf water content; CO_2 varies little with time so it is excluded from calculating leaf conductance. Canopy conductance is a function of the leaf conductance because the total canopy is a collection of individual leaves with an account for the area of the vegetated surface and the shelter factor.

Errors due to the uncertainty of the inputs into the model can be estimated through an error and sensitivity analysis. Ahn (1996) performed a sensitivity analysis on the Penman-Brusteart model and their correlated variables. Error was separated into 3 kinds: model error, propagated error from variables, and error due to parameters. The sensitivity analysis showed that the model was more sensitive to variables than to parameters, so the error due to parameters was negligible.

2.2.3 Streamflow

Streamflow (Q) is generally considered the most accurate variable in the water balance equation since it is readily measurable at a single location, the watershed outlet, with well established methods. Discharge can either be measured directly with field

equipment or computed from rating curves developed from previous discharge measurements.

Direct methods of measuring discharge are velocity-area gaging and dilution gaging. Velocity –area gaging directly measures the velocity and cross-sectional area of a river at numerous locations along the river. There are several different methods of measuring the velocity of the river, but the most popular are current meters. The velocity values are integrated to obtain the total discharge for the river. Dilution gaging uses a tracer to measure the velocity of the river.

A rating curve for a river is a relation of stage to discharge for a river. It is constructed from measuring stage for the river and direct measurements of discharge. Ideally, the rating curve covers all possible stages of the river. It is constructed from a number of years' worth of measurements to construct a reasonable curve for the river. The rating curve becomes an indirect method of determining discharge for a river; once the stage is measured, then the corresponding discharge is obtained.

Sources of error in the discharge measurements are measurement error due to the accuracy of the instruments being used, error due to timing (approximation uncertainty), and hysteresis in the stage-discharge relationship. Stream discharge varies continuously in time and measurements are instantaneous values taken at specific points in time. The time at which the measurement is taken and the temporal frequency can affect the value. The most important factors in quantifying errors in streamflow are the presence of a rating curve or stage-discharge relation for the water body in question, and the type of gage used to measure stage. A series of USGS papers for estimating errors in streamflow were all based on the method of streamflow gauging and the rating curve for the river.

Errors in streamflow values are cognitive errors in the form of human factors in measurement error. Moss and Gilroy (1980) found that uncertainty is a function of site visits to make discharge measurement and service recording equipment; whereas increased site visits decrease uncertainty in measurements. Anning (2002) agreed in that he found that the accuracy of streamflow data could improve by increasing the number of discharge measurements. For streamflow that was measured from a gage, Sauer and Meyer (1992) found that there are numerous components of the measurement error stemming from uncertainties in the measurements. They found that the standard error of discharge measurements ranged from 3-6%, but could be as low as 2% under ideal measurement conditions or as large as 20% when measurement shortcuts were taken. Moss and Gilroy assumed that for computed discharges the uncertainty came from error in the rating curve and devised a method that considered serial correlation of errors in the discharge rating shifts. Anning (2002) agreed with this idea but modified portions of their process to account for more recent methods to estimate the error in discharge measurements.

3 Methodology

3.1 Introduction

The goal of this research is to determine the water budget water balance closure and its accuracy using equation 1-2 by quantifying the components of the annual water budget for the Tom River basin and-- most importantly – the uncertainty in the components and the water balance closure using equation 1-3. Precipitation (P) and evapotranspiration (E) are spatially variable whereas streamflow (Q) is a point measurement in space for this basin. Based on this, the areal coverage of precipitation and evapotranspiration was needed to calculate the annual expected values (equation 1-1), the water balance closure (equation 1-2), and the uncertainty in each term (equation 1-3). Different methods of quantifying the components and their associated error were used. The methods of quantifying uncertainty depended on the available information on the processes, and the methods used to obtain the basin estimated average.

All data were arranged into water years, not calendar years. This was done to be consistent with the assumption of negligible change in storage. The water year begins October 1 of the preceding year and ends September 30.

3.2 Study Site

The Tom basin is a 57000 km^2 subbasin of the Ob River watershed located in the southwestern region of Siberia in Russia. The Tom River, 840 km long, flows north from the Alatau Range of the Altai Mountains and drains into the Ob River at the city of Tomsk. The elevation of the basin ranges from about 100 m to 3500 m. The region is

primarily steppe land used for agricultural purposes, mountainous region, and a heavily industrialized region **(see Figure 1.1).**

3.3 Precipitation

Kriging interpolation was used to estimate the annual basin average precipitation. In addition, kriging provided the standard error of the basin averages.

3.3.1 Description of Data

Precipitation gage data from the National Climatic Data Center (NCDC) formerly maintained and distributed by the National Snow and Ice Data Center (NSIDC) were used. The data set consists of monthly precipitation data from 622 stations located in the Former Soviet Union from the years 1891-1993. It also includes gage information such as elevation, latitude and longitude, and station names. For this analysis, 40 gages were used with 2 located within the basin and the other 38 located outside the basin. A mask of the Tom basin obtained from Saini (2002) was used to select the appropriate stations. Since only two stations were located within the basin, more had to be selected to achieve a more accurate estimate of precipitation; all stations within a 600-km buffer of the basin were selected **(Figure 3.1).** Data from 1980-1985 were used to make the precipitation consistent with the streamflow and evaporation data. From the monthly values, annual totals for each gage were produced, and this was the data set used for the estimation of variance in precipitation.
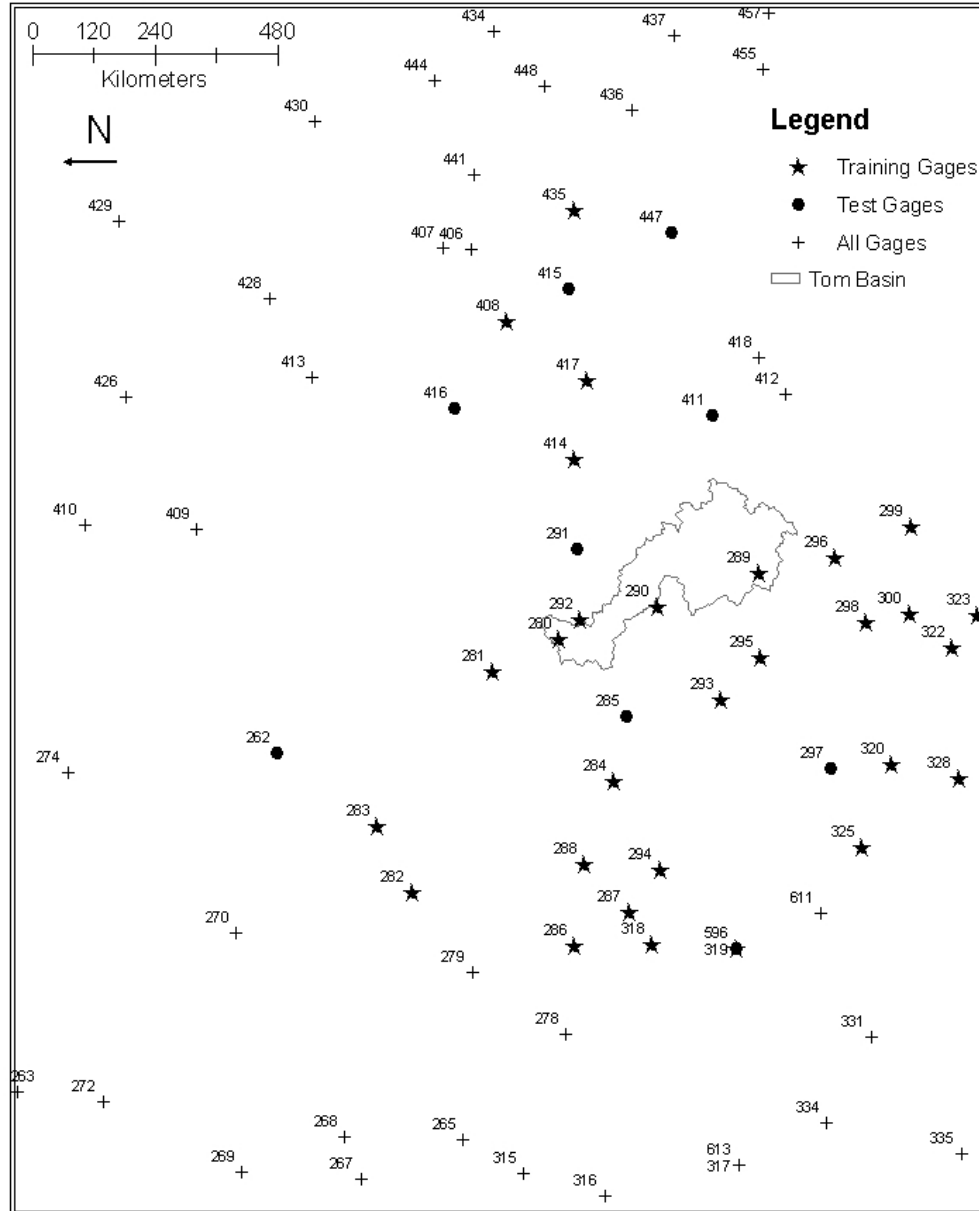
Figure 3.1 Precipitation gages in Siberia, Russia with outline of Tom River basin. Training set and test set of gages are shown. Map is in EASE grid projection.

3.3.1.1 Filling in Missing Values

Monthly precipitation values for some stations were missing during the period of

analysis. The missing values would introduce inaccuracies in the annual totals. The

normal station averaging method was used to fill in the missing values (Dunne et al.,

22

1978). This method was used to bypass the 10% within each value criterion needed for the station average method (McCuen, 1998). Three nearby stations were used to get the estimated amount of precipitation for the months in question.

$$P_A = \frac{1}{3}(\frac{N_A}{N_B}P_B + \frac{N_A}{N_C}P_C + \frac{N_A}{N_D}P_D) \qquad (3\text{-}1)$$

where P_B, P_C, and P_D are precipitation values for three surrounding stations during the gap at station A and N_A, N_B, N_C, and N_D are the long-term monthly averages.

3.3.2 Estimation of Annual Average Precipitation, $\overline{P}$

Orographic effects cause uncertainty in precipitation, so the data were tested for orographic effects by performing a regression analysis between elevation and average annual total of precipitation. A significant trend between elevation and precipitation for the gages used was not detected (**Figure 3.2**), so an orographic effect was not included in the analysis. Based on physical reasoning, such an orographic effect would be expected; the lack of a significant trend may be explained by the lack of gages at high elevations.
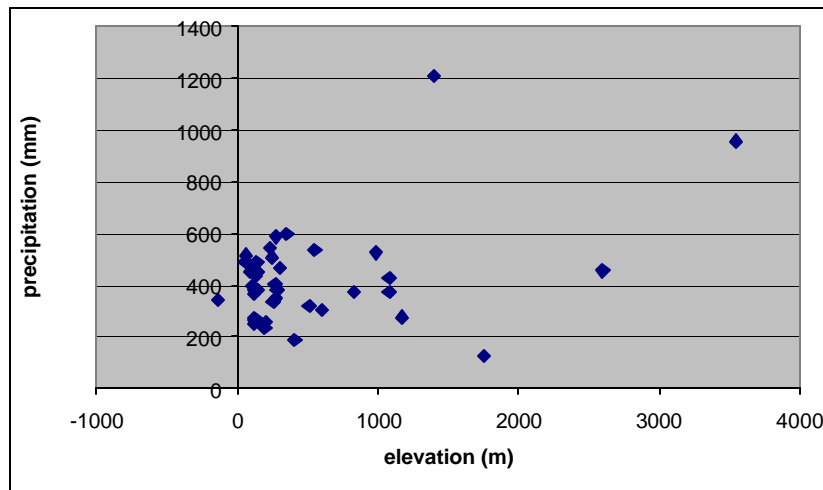
Figure 3.2 Plot of average annual precipitation (mm) for water years 1981-1985 versus elevation (m) of gages used for analysis

The Rosner outlier test was used to test for outliers in the data (**table 3.1**). The test

assumes that all data points are from the same normal distribution with a mean and

standard deviation.

Table 3.1: Rosner Outlier Test Results

water year	i	n-i+1	Mean (mm)	standard deviation (mm)	x	R	R_c	decision	Station
1981	1	41	365.96	192.43	1195.1	4.309	3.05	outlier	station 418
	2	40	345.24	141.10	641.2	2.098	3.04	no	
1982	1	41	376.78	195.56	1038.8	3.385	3.05	outlier	station 289
	2	40	360.23	166.45	890.1	3.183	3.04	outlier	station 418
	3	39	346.65	144.41	641.7	2.043	3.03	no	
1983	1	41	479.81	193.16	1216	3.811	3.05	outlier	station 418
	2	40	461.41	155.00	959	3.210	3.04	outlier	station 289
	3	39	448.65	134.07	689.7	1.798	3.03	no	
	4	38	442.30	129.80	667.7	1.736	3.01	no	
1984	1	41	438.15	188.46	1101.7	3.521	3.05	outlier	station 418
	2	40	421.56	157.66	1090.5	4.243	3.04	outlier	station 289
	3	39	404.41	115.90	674.7	2.332	3.03	no	
1985	1	41	487.71	251.10	1657.3	4.658	3.05	outlier	station 418
	2	40	458.47	169.45	1053.7	3.513	3.04	outlier	station 289
	3	39	443.21	141.09	769.8	2.315	3.03	no	

Note: Tested largest values of dataset consisting of 41 gages (n). Where i = the data point being tested, x is the value of the data point in mm, R is the computed test statistic, and R_c is the critical values at a 5% level of significance

 The results of this test showed that two stations, station 418 & 289 were outliers. The

annual totals of precipitation for these two stations were much higher than the other

stations. Station 289 could not be discarded from the dataset, because it was one of only

two of the stations located within the basin. Although shown to be a statistical outlier,

station 418 is one of very few stations at higher elevations, and could represent the true range of variability in the precipitation population. As a result two datasets were created: one with station 418 and one without station 418. All of the following procedures were separately performed on both datasets.

The precipitation data file was converted into a comma separated value (CSV) file in order to use it in ArcGIS. The data did not have spatial attributes, so these were defined using ArcToolbox. The data was converted to the EASE grid projection (Lambert Azimuthal Equal Area Projection). In this projection, every pixel represents an equal area on earth. This is important for the polar regions because of the areal distortion caused by the convergence of the lines of longitude at the poles. The Cartesian coordinates for the stations were given using a XY tool downloaded from ArcObjects online source of add-ons for ArcGIS. The stations were mapped using the x and y fields by the display events tool. The mapped stations were then converted into a shapefile.

3.3.2.1 Developing Semivariograms

Kriging was the interpolation method chosen to estimate the areal distribution of precipitation across the basin. In addition to being a recommended interpolation method (Dingman, 1998), kriging can provide the standard error of the interpolated estimates; this information is used in quantifying uncertainty in the basin precipitation (below). In order to use kriging, a semivariogram had to be developed. A semivariogram describes the spatial autocorrelation of data. Spatial autocorrelation is the likelihood that values of a parameter are related the closer they are located to each other. The spatial correlation decreases with increasing separation distance. The autocorrelation is calculated as the variance between the points with respect to distance. The

semivariogram graphically represents the variance of the values as a function of distance between the points. The variance of the points are binned where the variance of points within a certain distance of each other are averaged together to get the semivariance for that range of the data. The binned raw semivariance becomes the experimental semivariogram of the data. The semivariogram has two parameters: the range and sill. The range is the maximum distance between the points where they are related to each other. Points separated by a distance greater than the range are said to be independent of each other, and at this distance the semivariance becomes a constant that is equal to the sample variance. The constant value is the sill or the maximum semivariance between the points. The experimental semivariogram is fit by a theoretical semivariogram, which is a function that best describes the shape of the semivariance.

Spherical semivariograms were chosen to model the data. The equation for a spherical semivariogram is as follows (Deutsch et al., 1998):

$$\begin{aligned} \boldsymbol{g}(r) &= s\left(\frac{3r}{2h} + \frac{1}{2}\frac{r^3}{h^3}\right) \qquad & r \le h \\ & & r \ge h \\ \boldsymbol{g}(r) &= s \end{aligned} \tag{3-2}$$

where h is the range, s is the sill, and r is the separation distance. Spherical and exponential semivariograms are the most popular types to use, but the spherical model was chosen because it has a more defined sill. The goodness of fit of the spherical semivariograms was determined through a numerical optimization program (McCuen, 1993). The program optimized the sill and range of the semivariograms based on the objective function of minimizing the sum of the squares of the prediction errors. The values of the sill and range were compared to those given by the ArcGIS geostatistical program, and their prediction abilities were compared.

The effects of the number of stations used was tested. Semivariograms were calculated separately for a 400 km, 500 km, and 600 km buffers, created from a buffer tool in ArcMap, to evaluate the effect of the increased number of points **(Figure 3.3)**. The stations within each of the buffers was selected and then converted into a separate shapefile for ease of computing semivariograms. The semivariograms for the three buffers did not vary much, with all three having similar ranges and sills (**Table 3.2**).
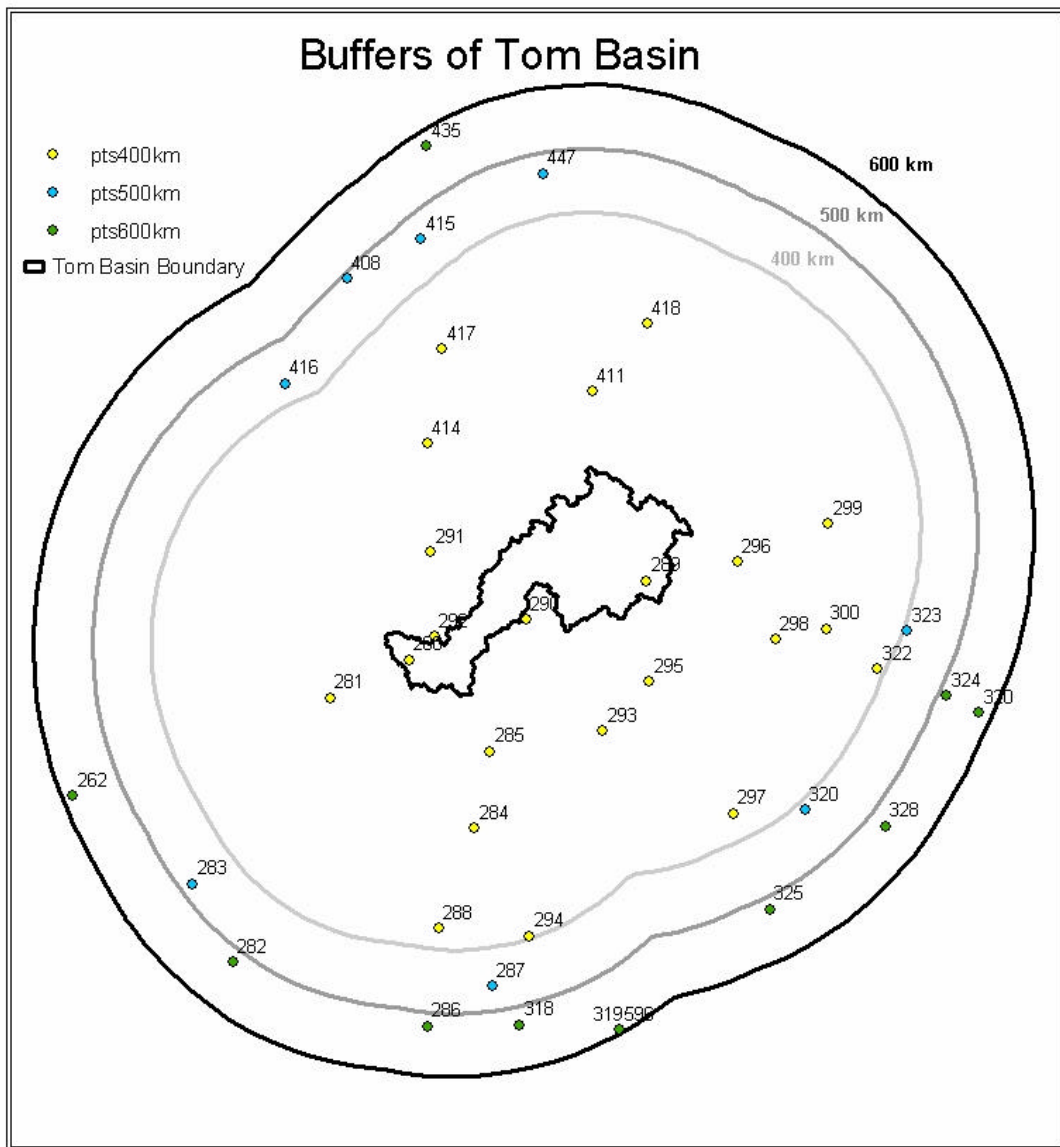

Figure 3.3: Map of Tom Basin surrounded by three buffers at distances of 400, 500, and 600 km away from basin. Gages within each buffer are shown in different colors.

Table 3.2: Semivariogram Parameters for buffers 400-600 km

buffer distance (km)	400	500	600
lag size (m)	56958	56958	56958
number of lags	12	12	12
nugget	0	0	0
Range (m)	279930	279940	302760
Sill (mm^2)	25325	22147	21072

The points within a 600 km radius of the watershed were used for the analysis because the increased amount of points gave more confidence in the prediction model.

3.3.2.2 Kriging Prediction Models

All kriging procedures were performed using the geostatistical extension in ArcGIS. Separate analysis was performed for each year of data. The precipitation data for each shapefile was the input data for the kriging analysis. The data were separated into a test and training set for validation using a tool to create data subsets in the program. The model would be calibrated using the training set and then validated using the test set. The test set consisted of 10 randomly selected points from the entire data set, while the training set consisted of the remaining 30 points. Determining the optimal parameters to produce the best-fit kriging map required subjective judgment as follows: decisions about the type of kriging, trend removal, search neighborhood, and anisotropy had to be made. The process includes four steps: geostatistical methods, semivariogram model, search neighborhood, and cross validation **(Figures 3.4-3.8)**. Geostatistical methods included kriging type, trend removal, and type of map. For all analyses an, "ordinary kriging prediction map" was the type used; since orographic effects were not evident in the data, it was not necessary to model a trend or transform the data. Inputs for the semivariogram calculation were the semivariogram type, lag size, and number of lags.
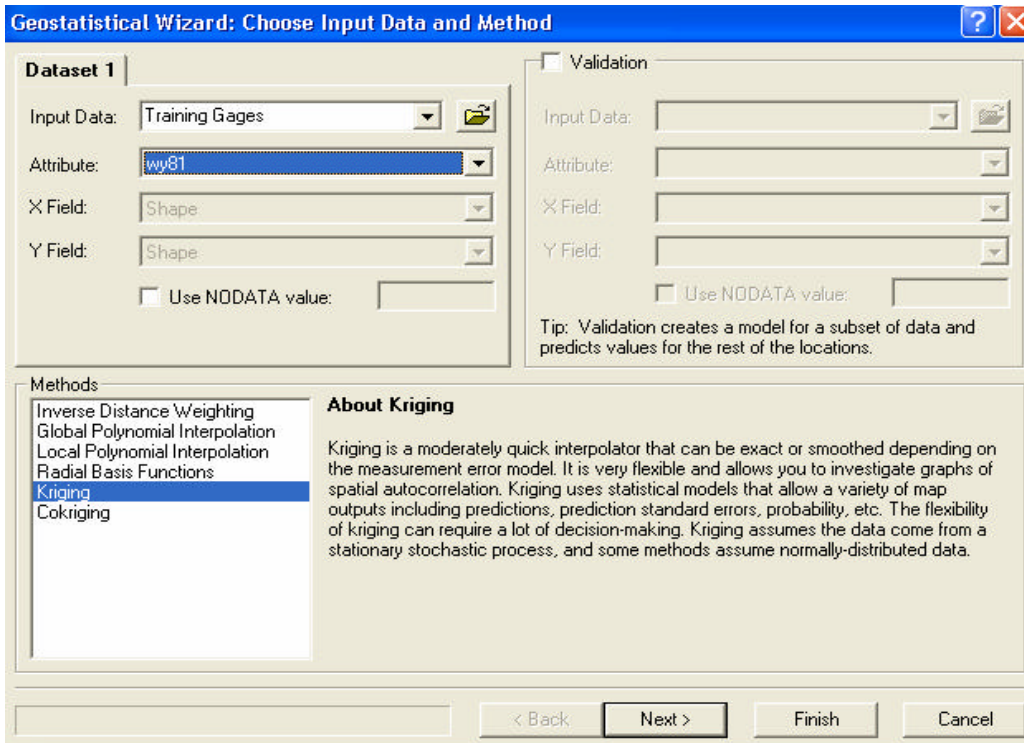
Figure 3.4: Screen capture of input data selection step. Step includes input data file, selection of information from its table of data to be used for interpolation method, type of interpolation method, and if validation will be used.
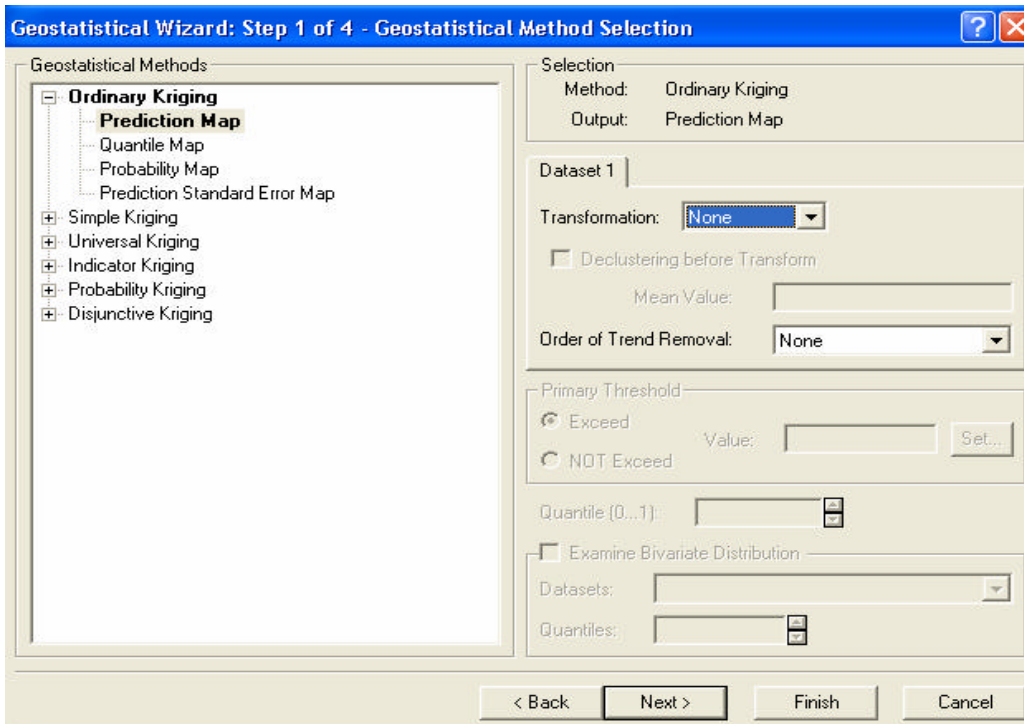
Figure 3.5: Screen Capture of Geostatistical wizard step one. Step includes decisions on type of kriging used, transformation and trend removal options.

29
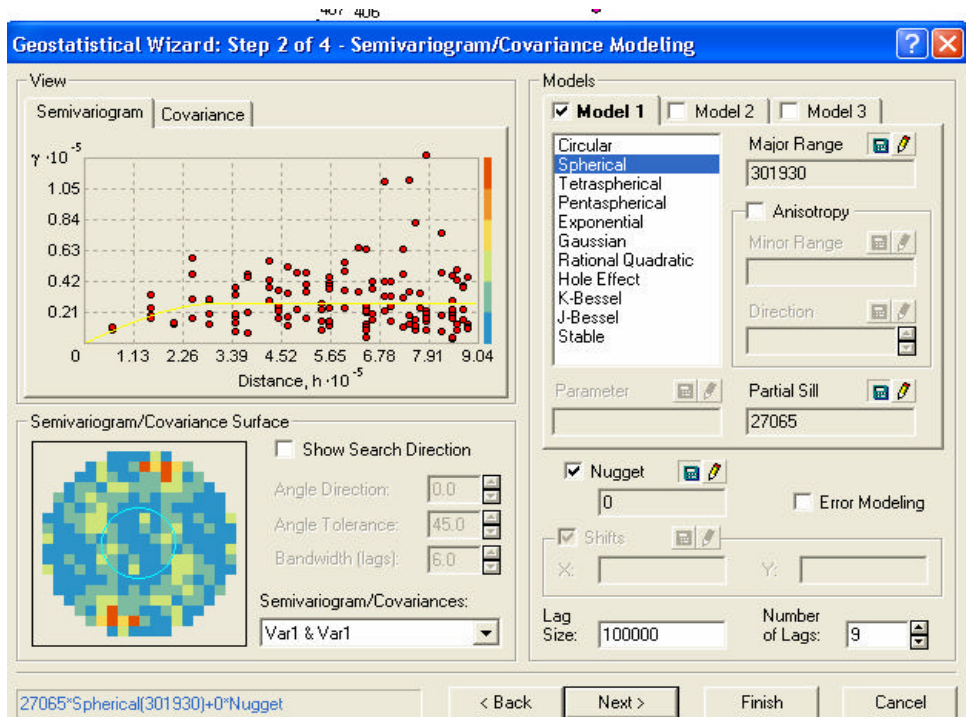
Figure 3.6: Screen capture of step 2 of geostatistical wizard. Step includes type of semivariogram and its parameters, display of either semivariogram of covariogram, and search direction and weights of points in search surface. Parameters can either be calculated by the program or input by the user.
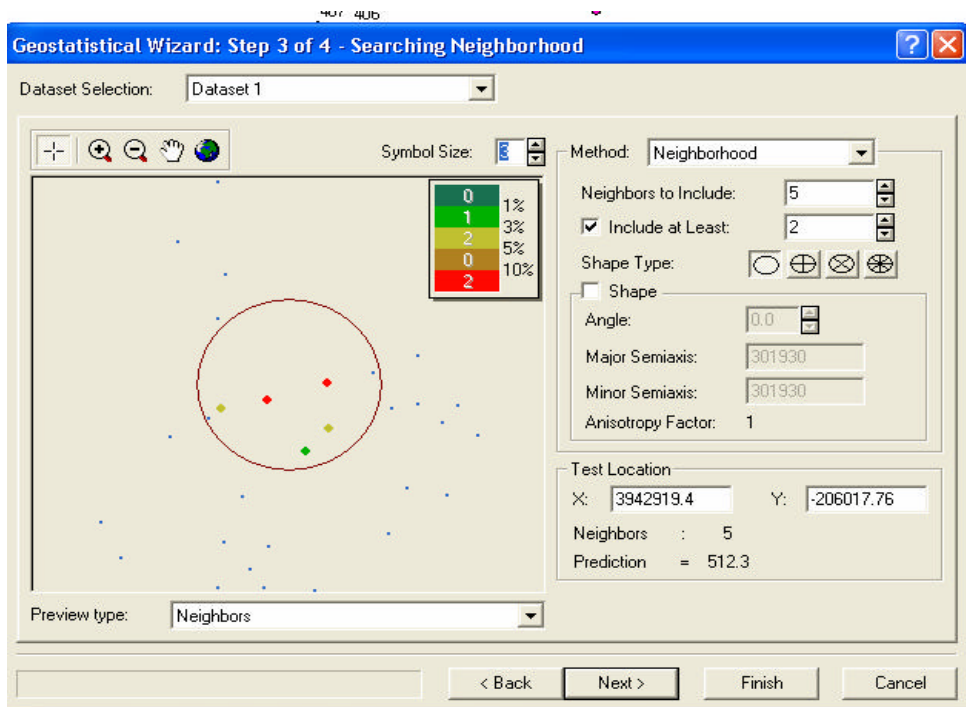
Figure 3.7: Screen capture of step 3 of geostatiscal wizard. Step includes number of points in search radius and search neighborhood shape. It also shows search neighborhood for a particular location and the weights of points within radius.
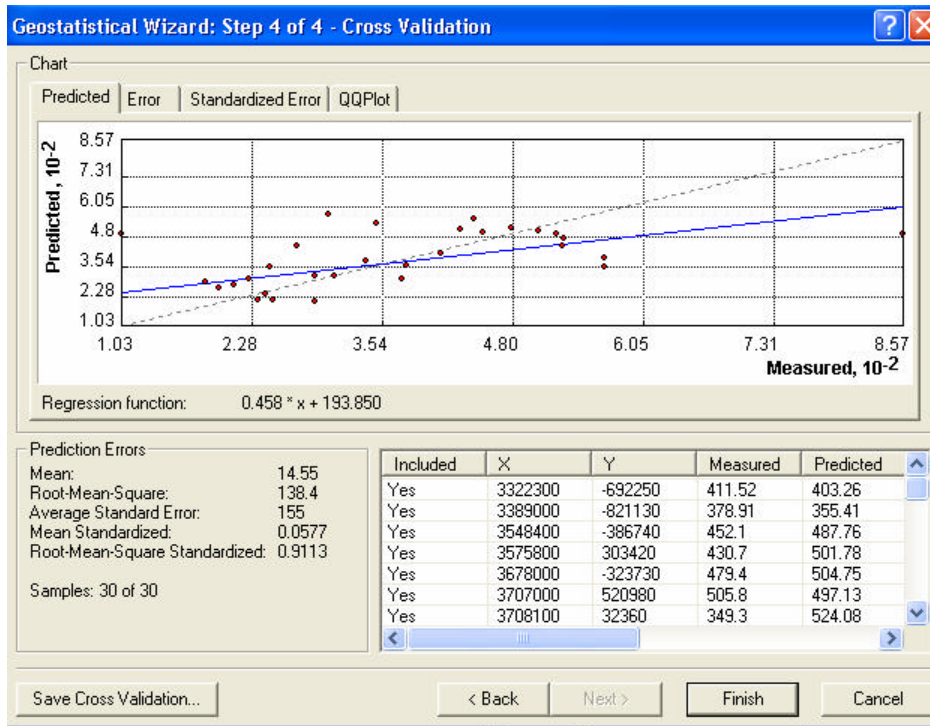
Figure 3.8: Screen capture of step 4 of the geostatistical wizard. This step is the cross-validation phase of the interpolation method. It uses every point in the data set to validate the model. Each point is removed from the data set and the model is used to predict that point. The model statistics are given, as well as plots to demonstrate the prediction capabilities of the model.

The same lag size and the number of lags used in the NUMOPT program were selected to allow comparison between the two semivariograms: the ones calibrated from NUMOPT and the ones calibrated within the geostatistical program. The program optimized the range, sill, and nugget based on least squares regression for each chosen lag size and number of lags. Anisotropy was not modeled, and the search radius was a circle with no divisions because the data had no spatial trends. The initial search neighborhood was a minimum of two points and a maximum of five points within the search radius. This was changed once the basic parameters of the semivariogram were chosen. The final decision for the parameters was made based on the goodness-of-fit statistics such as root mean

square standardized, bias of errors, mean error, standard error ratio, and overall fit of prediction map all given from the cross validation results.

Once the semivariogram parameters were fitted, the sensitivity of the model to the search neighborhood was investigated. The search neighborhood always contained a minimum of two gages, but the amount was increased from a minimum of two gages within the search radius to the maximum number of gages where a change in the prediction model was not observed. A change in the prediction model was defined as the point where the goodness-of-fit statistics changed. The maximum number of gages to use in the search neighborhood for the model was determined by the amount required to give the lowest standard error ratio.

Once all the parameters were determined, the semivariogram was used to create the prediction and standard error maps. The models for the analysis set without station 418 were validated to ensure their accuracy. The validation was performed on the test data set. Error analysis was performed to determine the quality of the prediction model. The error analysis was a graphical check for local bias in the prediction values and statistics on the error values.

3.3.3 Estimation of Uncertainty in Annual Average Precipitation, $S^2(\overline{P})$

The standard error maps created by the ArcGIS Kriging routine were converted into raster datasets (grids) with a grid cell resolution of 1 km^2. The Tom basin shapefile was converted into a grid for use as a mask for the standard error maps. Raster calculation was performed to multiply the Tom basin by the standard error map to obtain a map displaying the standard error only in the Tom basin. The calculation grid was a

temporary file, so it was exported as a permanent grid. The grids were converted into ASCII text files to use as input into the total variance program.

The total variance program was developed in FORTRAN, based on the total variance of a linear function theory. The program calculated the total standard error of the estimates of the estimated precipitation in each grid cell and the covariance between pair of grid-cell precipitation estimates. The covariance was based on the same spherical semivariogram used to estimate the precipitation distribution across the basin (Deutsch et al., 1998):

$$C = s \cdot \left(1 - \frac{3r}{2h} + \frac{1}{2}\frac{r^3}{h^3} \right)$$

(3-3)

where s is the sill of the semivariogram, r is the separation distance between points, and h is the range of the semivariogram. The program calculated the separation distance between all cells, noting that at any separation distance greater than the range (h), the covariance becomes zero (in other words, beyond the range of the semivariogram, the estimated precipitation values are independent of each other). The input into the program was the ASCII text file of standard errors, and the sill and range of the semivariogram used for kriging. The program calculated the number of cells and the separation distance between each pair of cells and then calculated the total variance (Mendenhall et al., 1995):

$$S_{tot}^2 = \frac{1}{n^2}\left(\sum_{i=1}^{n} S^2(i) + 2\sum_{i=1}^{n}\sum_{j=i+1}^{n} Cov(i,j) \right)$$

(3-4)

where S_{tot}^2 the total variance, n is the number of pixels, and S is the standard error of the estimated precipitation in pixel *i*, and Cov(i,j) is the covariance of precipitation between pixels *i* and *j*.

3.4 Streamflow

Streamflow is a point measurement, which was taken as the basin average. A literature based estimate to quantify uncertainty in the basin average streamflow was used.

3.4.1 Description of Data

Streamflow data were obtained from the University of New Hampshire R-Arcticnet Hydrological Data Group. The data set consists of average monthly discharge given in m³/sec for 1918-2000 for the Tom River at Tomsk river gage site. The gage is 137 m above sea level located at 56.43N and 84.97E. Data from 1980-1985 were used so that this dataset would be compatible with the other two datasets.

3.4.2 Estimation of Annual Average Streamflow, $\overline{Q}$

The average monthly streamflow for the measurement site was given in m³/sec. These data were divided by the basin area to convert into monthly depths of flow in mm. The monthly values were summed to get the average annual depth of flow.

3.4.3 Estimation of Uncertainty in Annual Average Streamflow, $S^2(\overline{Q})$

The analysis was limited by the lack of a rating curve for the Tom River. Based on literature reviews, an error of 5% of average annual streamflow was assumed (Winter, 1981).

3.5 *Evapotranspiration*

The basic method was a derived distribution of evapotranspiration values based on Monte Carlo simulation of the Penman-Monteith equation. This gave the estimated expected E and variance of the estimate.

3.5.1 Description of Data

Evapotranspiration values, as well as the input variables used to compute evapotranspiration, were supplied by the NASA group as output from PRMS model based on the Penman-Monteith equation. The Tom basin was divided into 19 hydrologic response units (HRU's) as a premise for the PRMS model. The evapotranspiration values were given in inches in 3-hour increments daily for the years 1980-1985 for each of the HRU's. The basin-average evapotranspiration was calculated as an area-weighted average of the values for each HRU. This mean was used as a check for the mean obtained from the derived distribution method described below. The NASA group also supplied the area of each HRU in square kilometers and acres.

Values of the input variables required by the Penman-Monteith equation were given for Tomsk (elevation 137 m above sea level). The inputs obtained from the NASA group were air temperature (T_a) in °C, incoming clear-sky solar radiation (K_{cs}) in MJ m^{-2} day^{-1}, cloud ratio (C), wind speed (v_a) in m/s, relative humidity (W_a), and atmospheric pressure (P) in kPa, all measured at Tomsk. Taken at the lowest point in the watershed, these measurement may not be representative of the whole basin, but they are the only meteorological observations available.

The surface temperature at Tomsk (required for calculating net radiation) was estimated as the 24-hour average of the reported air temperatures. The heat capacity of air and the density of water were constants in the model at 0.001 MJ kg^{-1} K^{-1} and 1000 kg m^{-3} respectively.

Because measurements of soil moisture were not available, a model was developed for soil moisture deficit, assuming exponential drainage from saturation after a rainfall event. The model was developed through approximation by inspection of soil moisture discharge curves in Dingman (1994):

$$\Delta q = \Delta q_{max}(1 - e^{-bt}) \qquad\qquad (3\text{-}5)$$

where $\Delta\theta$ is the soil moisture deficit (cm), $\Delta\theta_{max}$ (cm) is the difference between saturation water content and field capacity, t (days) is the time since the last rain, and β (days^{-1}) is a time scale. Saturation water content and field capacity were estimated based on knowledge of the soil texture in the Tom basin. The time scale was estimated by examining known soil drainage time series for soils similar to those found in the basin.

3.5.2 Estimation of Annual Average Evapotranspiration, $\overline{E}$, and its Uncertainty, $S^2(\overline{E})$

The annual average and standard deviation of E were calculated for each water year from a derived frequency distribution of E. A derived frequency distribution can be describes as:

> A function of random variables x and y, g(x,y), is itself a new random variable. The expected value of g(x,y) may be found directly…without ever determining the PDF f(g). However, if we have an interest only in the behavior of random variable f and we wish to answer several questions about it, we may desire to work…with the PDF f(g). A PDF obtained for a function of some random variables whose PDF is known is referred to as a derived PDF (Drake, 1988).

E is a nonlinear function of many variables, and analytical determination of its derived distribution would be tedious; therefore, a Monte Carlo method was used. The frequency distribution of E was developed by simulation, using the Penman-Monteith equation. A value of E was calculated for each 3-hour time step at each of 1000 simulated locations in the basin. Characteristics of the simulated locations were assigned by a combination of physical theory and random sampling. The steps in creating the derived distribution of E are described in the following sections. The E values were in mm/s-3hr so the resultant statistics were converted into mm.

3.5.2.1 Distribution of Variables

Elevation. The gamma distribution was the assumed distribution of elevation determined from information from Saini (2003) (**Figure 3.9**). The mean and standard deviation of elevation had to be inferred by inspection of the elevation histogram, since the actual numbers were not available due to computer system failure. The gamma probability density function is

$$f(x) = \frac{\lambda^{\alpha} x^{\alpha-1} e^{-\lambda \cdot x}}{\Gamma(\alpha)} \tag{3-6}$$

where x in this case is elevation (m) in the basin, λ is the scale parameter, α is the shape parameter, and Γ is the gamma function. The parameters for the gamma distribution were calculated based on the method of moments, which uses the assumed mean and standard deviation.

$$\beta = \frac{s^2}{\bar{x}} \tag{3-7}$$

$$a = \left(\frac{\bar{x}}{s} \right)^2 \tag{3-8}$$

where $\bar{x}$ is the mean of the elevation, and s^2 is the standard deviation of elevation. The mean and standard deviation were assumed to be 500 m and 375 m^2, respectively. Elevations of the 1000 simulated points were sampled from this distribution.
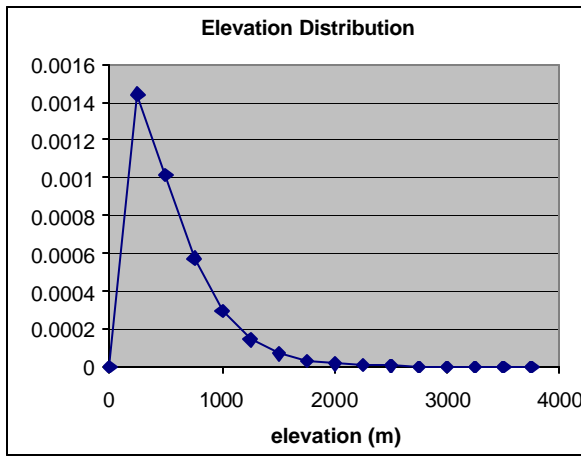
Figure 3.9: Gamma distribution of elevation in basin.
Mean = 375 m and standard deviation = 500 sq m

Temperature and Pressure. The elevation distribution was then used to assign the temperature and atmospheric pressure for the simulated points. Temperature and atmospheric pressure both decrease with increasing elevation. Both can be modeled as a linear change with elevation. The linear rates of decrease are called lapse rates. The temperature lapse rate is commonly called the environmental lapse rate, and the pressure lapse rate is commonly called the scale height of the atmosphere. The air (a) and surface (s) temperature model is

$$T_{a,s} = (T_{a,s})_m - \Delta T \cdot (Z - Z_m) \tag{3-9}$$

where $T_{a,s}$ are the temperature of the subscript type at the simulation point, $(T_{a,s})_m$ are the temperatures of the subscript type at the measurement site, the temperature lapse rate, $\Delta T = 0.65\ °C/100$ meters (Dingman, 2002), Z is the elevation of the simulation point in meters, and Z_m is the elevation of the measurement point, Tomsk, at 137 m. The pressure model is

$$P = P_m - \Delta P \cdot (Z - Z_m) \tag{3-10}$$

where P is the atmospheric pressure at the simulation point, P_m is the atmospheric pressure at the measurement site, and the standard atmosphere lapse rate, ΔP, is taken as 0.0125 kPa/m (Wallace and Hobbs, 1977).

Vegetation Type and Parameters A multinomial distribution was assumed for vegetation type, where the probability assigned to each type was proportional to the areal coverage of each across the basin (**figure 3.10**). The vegetation type and areal coverage of each was obtained from Saini (2003). The three main types of vegetation in the basin are conifer, savannah, and cropland. The probably mass function of the vegetation type is

$$P_{x_1 x_2 x_3} = \frac{n!}{x_1!x_2!x_3!} p_1^{x_1} p_2^{x_2} p_3^{x_3} \tag{3-11}$$

where p_i are the probabilities of conifer, savannah, and cropland which are 0.7116, 0.0831, and 0.2053, respectively. It would have been preferred to have a land use map of the region, but since this was unavailable, the multinomial distribution was the next best approach to estimating the vegetation distribution conditional on elevation.
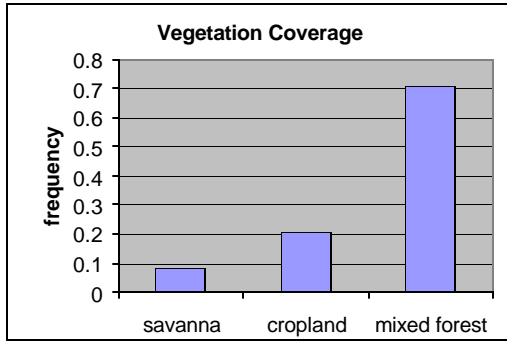
Figure 3.10 Vegetation distribution in basin

The following canopy characteristics were estimated based on the vegetation type and season: maximum leaf conductance, LAI, albedo, and vegetation height. Each of these was sampled from uniform distributions, whose limits were based on the type of land cover (**figures 3.11-3.14**). The limits of the distribution varied for each time period and plant type. The uniform distribution probability density function is

$$f(x) = \frac{1}{b-a} \tag{3-12}$$

where a and b are the lower and upper limits of the distribution, respectively. The mean and range of those distributions were given typical values based on land cover, as found in the literature (Dingman, 2002). The seasons for the vegetation parameters were determined based on biological information. The vegetation seasons were determined by the land types' "green-up" and "green down" periods of the land types (www.globe.com). Conifer land type was not assumed to have seasonal variation, but cropland and savannah were. The dormant season, or "green down", period was taken as September 1-April 30, and the active season, or "green up," was May 1-August 31. For each simulation point, the vegetation type selected from the multinomial distribution dictated which uniform distribution was used to simulate the vegetation properties for that location.
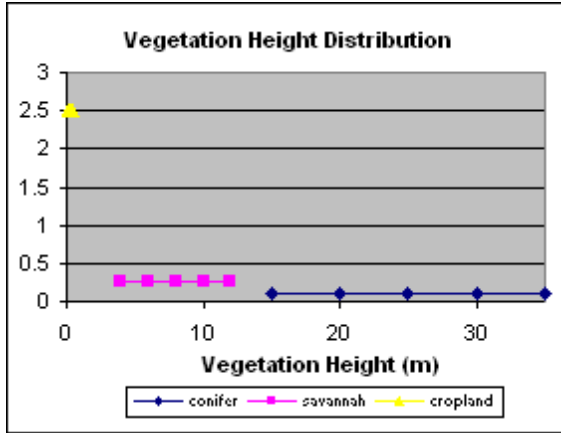
Figure 3.11: Uniform distribution of vegetation height (Zveg) for the 3 vegetation types
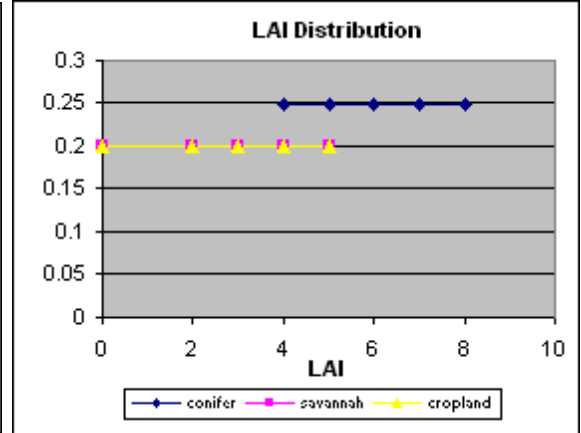
Figure 3.12: Uniform distribution of Leaf Area Index (LAI) for the 3 vegetation types
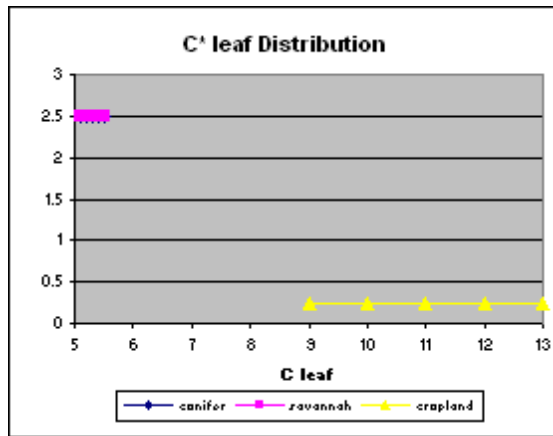
Figure 3.13: Uniform distribution of Maximum Leaf Conductance (C* leaf) for 3 vegetation types
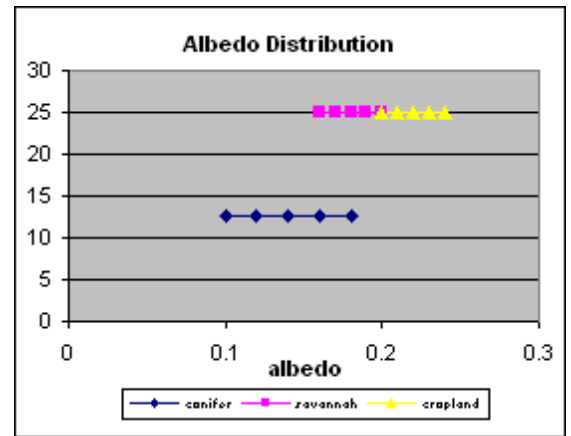
Figure 3.14: Uniform distribution of albedo (a) for the 3 vegetation types

The shelter factor was modeled based on its relationship with LAI. The shelter factor typically ranges from 0.5 to 1 and decreases with increasing LAI (Dingman, 2002). The proposed model was (**Figure 3.15**)

$$f_s = \begin{cases} 1 & 0 \leq LAI \leq 3 \\ 1 - \dfrac{1}{6}(LAI - 3) & 3 \leq LAI \leq 6 \\ 0.5 & 6 \leq LAI \leq 8 \end{cases} \tag{3-13}$$
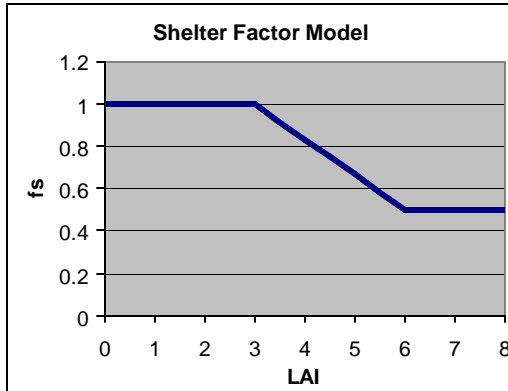
Figure 3.15: Shelter factor (f_s) model for the defined
Range of Leaf Area Index (LAI)

Cloud Cover. Frequency histogram analysis of the observed cloud ratio in time was performed to propose a distribution of the input. Using the cloud cover time series obtained from the NASA group, the average for the water years 1981-1985 was found and each daily value was subtracted from the average to remove the annual cycle. These deviations were plotted as a time series for each water year (**Figure 3.16**). The variability in the time series was used to distinguish between seasons instead of using the calendar seasons following the reasoning that cloud cover was expected to vary differently during different times of the year. The seasons for cloud cover were determined by inspection of the plots. The seasonal periods for cloud cover were October-April and May-September.

Because cloud cover is defined as a number between 0 and 1, the beta distribution is a convenient choice to describe this variable (**Figure 3.17**)

(a)

(b)

(c)

43
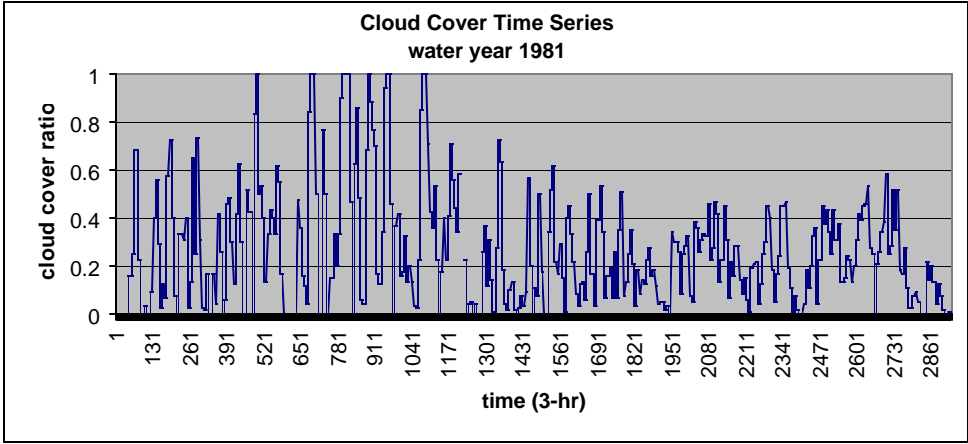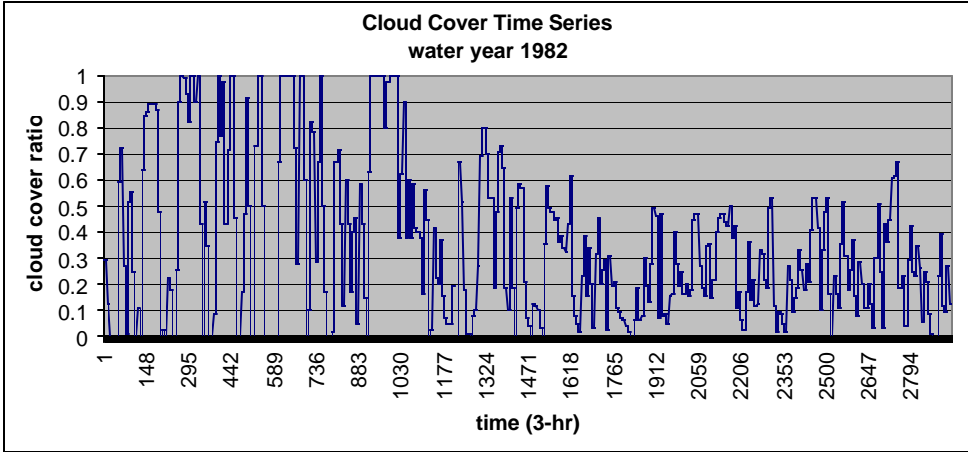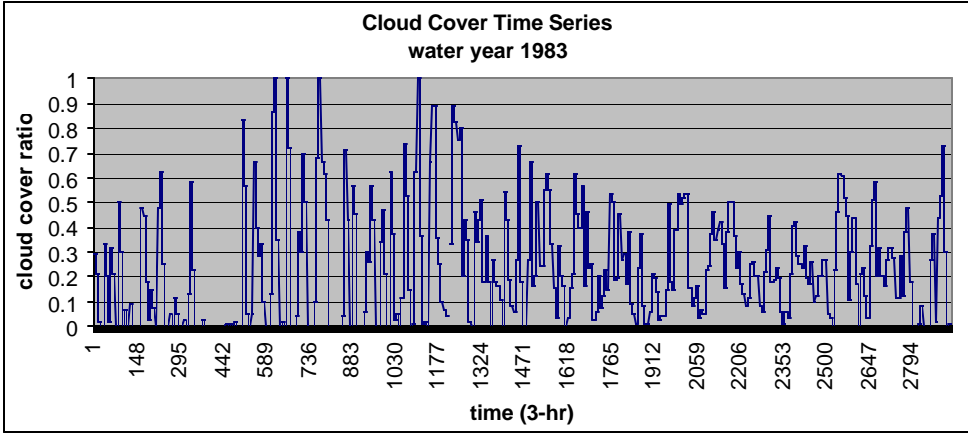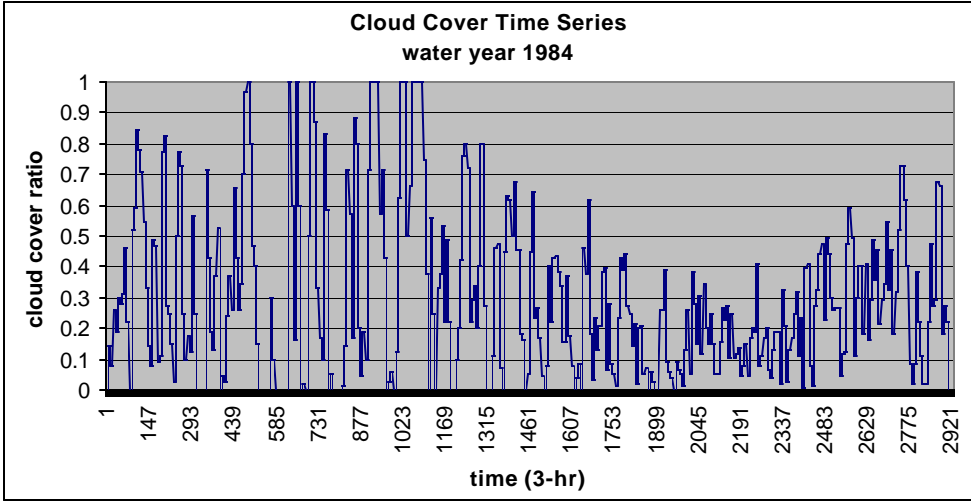
(d)
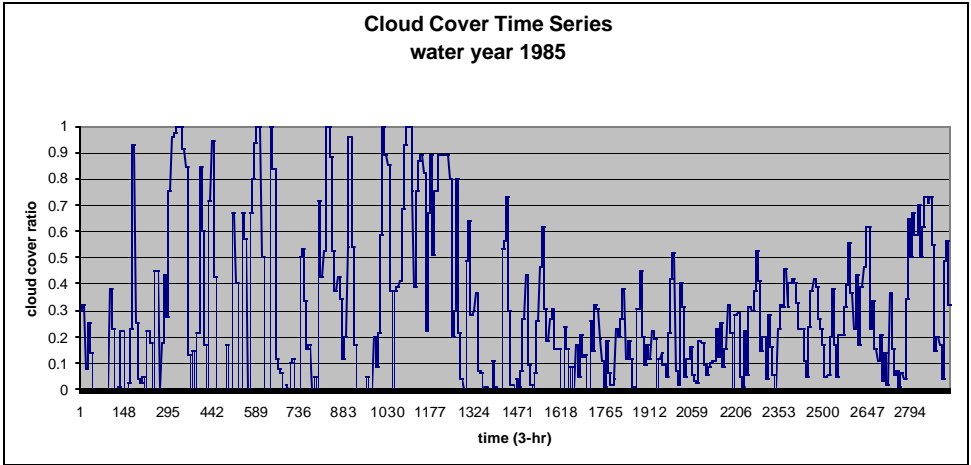
(e)
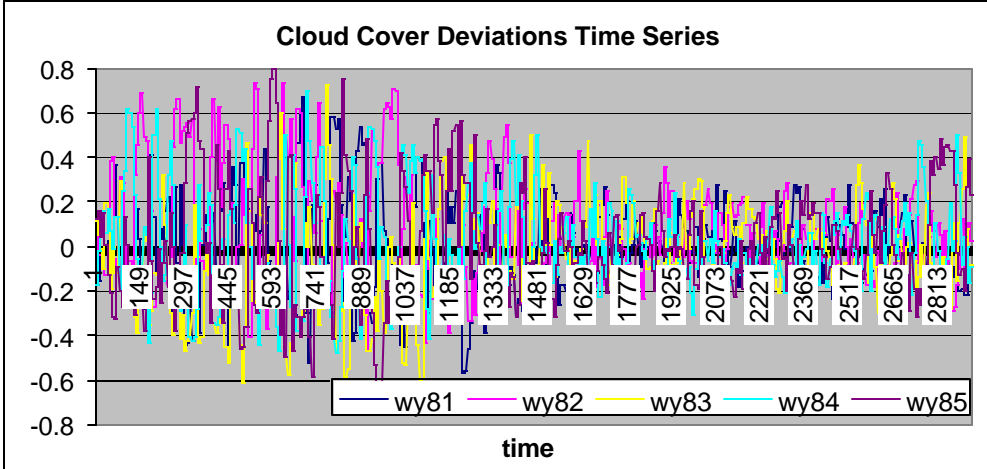
(f)

Figure 3.16(a-e) Times Series of Cloud Cover for each water year. Figure 3.16(f) shows the deviation of the time series from the 5-yr average.

44
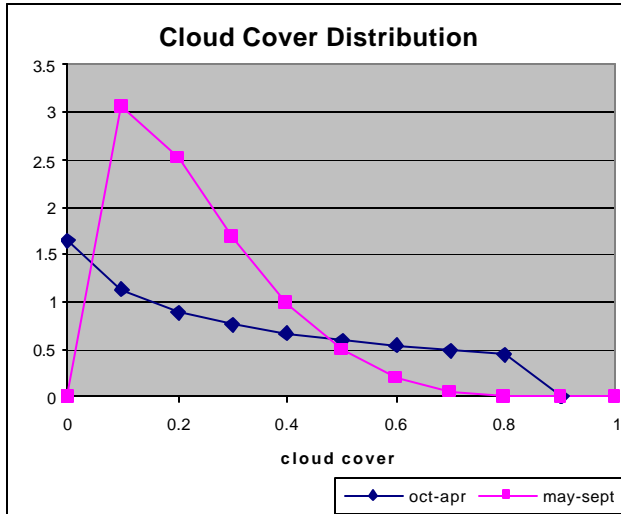
Figure 3.17: Gamma distribution of cloud cover
For time periods, Oct-Apr & May-Sep

The beta probability density function is

$$f(x) = \frac{x^{a-1}(1-x)^{b-1}}{B(a,b)}$$

(3-14)

where α is shape the parameter, β is the scale parameter, and $B(\alpha,\beta)$ is the beta function. The chi-squared goodness-of-fit test was performed on the proposed distribution to test if the assumption was appropriate (**table 3.3**). The results showed that the beta distribution was not appropriate to model cloud cover in time; however, due to the need of a spatial distribution and the physical limits of cloud cover, the beta distribution was used.

At each time step, cloud cover for each simulation point was simulated by sampling from a beta distribution with the mean equal to the observed cloud cover at

45

Table 3.3: Chi-Squared goodness-of-fit test results on the beta distribution for Oct-Apr during water year 1981

xl	o	cum p	p	e	(o-e)^2/e
0	288	0	0	0	0
0.05	176	0.260715	0.260715	442.1721	160.2263
0.1	88	0.3583	0.097585	165.5041	36.29451
0.15	128	0.431335	0.073036	123.8684	0.13781
0.2	144	0.491844	0.060508	102.6221	16.68383
0.25	72	0.544406	0.052562	89.14596	3.297783
0.3	64	0.591346	0.04694	79.60943	3.060622
0.35	112	0.634029	0.042683	72.39064	21.67271
0.4	104	0.673338	0.039309	66.66792	20.90487
0.45	64	0.709879	0.036541	61.97387	0.066241
0.5	96	0.744089	0.03421	58.0197	24.86229
0.55	48	0.776291	0.032202	54.61521	0.801261
0.6	40	0.806732	0.030441	51.62816	2.619
0.65	48	0.835601	0.028869	48.96187	0.018896
0.7	24	0.863043	0.027442	46.54153	10.91757
0.75	40	0.889166	0.026123	44.30475	0.418259
0.8	16	0.914044	0.024878	42.1933	16.26062
0.85	24	0.937713	0.023669	40.1421	6.491125
0.9	24	0.960151	0.022438	38.05559	5.191346
0.95	8	0.981215	0.021064	35.72394	21.51546
1	88	1	0.018785	31.85925	98.92838

Note: mean and standard deviation of cloud cover for time period of analysis were 0.302 & 0.289, respectively. xl is the limit of the interval, o is the observed frequency, cum p is the cumulative beta probability, p is the probability of occurrence, and e is the expected frequency. The total observed data was 1696 and the total test statistic was 450.

Tomsk and the variance was based on a seasonal analysis. The parameters for the beta distribution were calculated from the mean and standard deviation of the measurement site using the method of moments.

$$a = \bar{x} \cdot \left(\frac{\bar{x} \cdot (1 - \bar{x})}{s^2} - 1 \right) \tag{3-15}$$

$$b = (1 - \bar{x}) \cdot \left(\frac{\bar{x} \cdot (1 - \bar{x})}{s^2} - 1 \right) \tag{3-16}$$

In the beta distribution, high variances are not compatible with very low or very high means. The highest variance possible for the beta distribution is when alpha and beta

= 0. When alpha equals beta, the mean is 0.5. As the mean approaches either 0 or 1 (highly skewed beta distribution), the variance must become small. Analysis demonstrates that the variance for the beta distribution must be less than or equal to the mean for $\mu < 0.5$, and less than or equal to (1- mean) for $\mu > 0.5$.

The observed seasonal variance was used as a maximum possible variance for the simulated cloud cover. When the observed mean was either quite high or quite low, the variance was assigned as the minimum value of the following three choices:

$$s^2 = \begin{cases} \text{calculated seasonal variance at measurement point} \\ (1-\mu)^2 \\ \mu^2 \end{cases}$$

This analysis was based on forcing the beta function as the spatial cloud cover distribution, even though it was not well supported by time-series observations. This was a necessity of choosing a distribution from which to sample for Monte Carlo simulation. If the measured value of cloud cover was either 1 or 0, the simulated cloud cover was set equal to the mean.
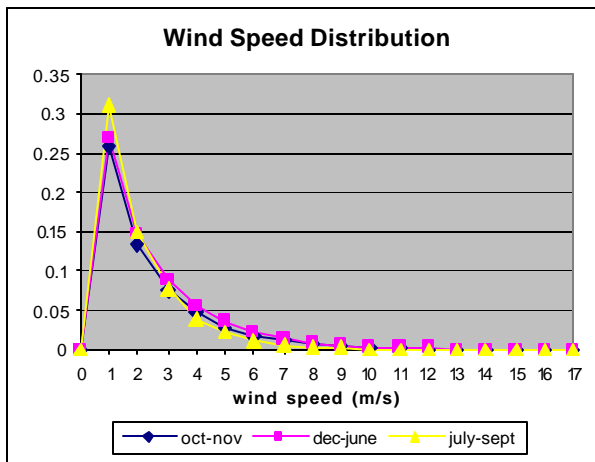
Figure 3.18: Gamma distribution of wind speed for time Periods, Oct-Nov, Dec-Jun, & Jul-Sep

Wind Speed. Wind speed at each point was sampled from a gamma distribution (**Figure 3.18**). The parameters were calculated using equations 3.7 and 3.8. The mean for each time step was the measured wind speed at the measurement site, and the standard deviation was the standard deviation of the measurement site for the appropriate time period, as determined by time-for-space substitution in analysis of the measured data, similar to the approach used with cloud cover. The seasonal periods for wind speed were October-November, December-June, and July-September (**Figure 3.19**). When the measured wind speed was 0.2, the lowest reported value, the simulated value was set equal to the mean, the measured value due to numerical issues in inverting the distribution for very low values.

Soil Moisture Deficit. Soil moisture deficit was calculated using equation 3.5 at the measurement site (**Figure 3.20**). For the simulation points, it was generated from the uniform distribution. The lower limit was zero and the upper limit was the value at the measurement site.
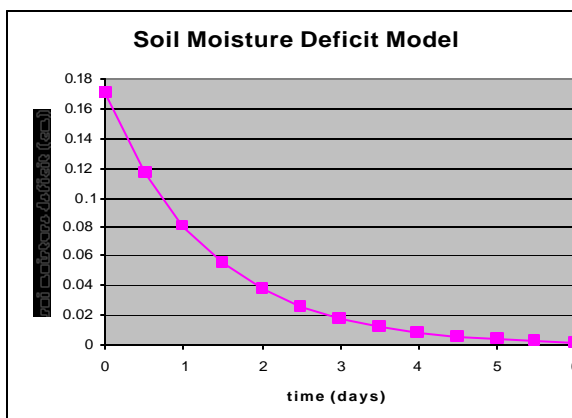
Figure 3.20: Soil moisture deficit model, where beta is 0.75 days^{-1}

(a)

(b)

(c)

49
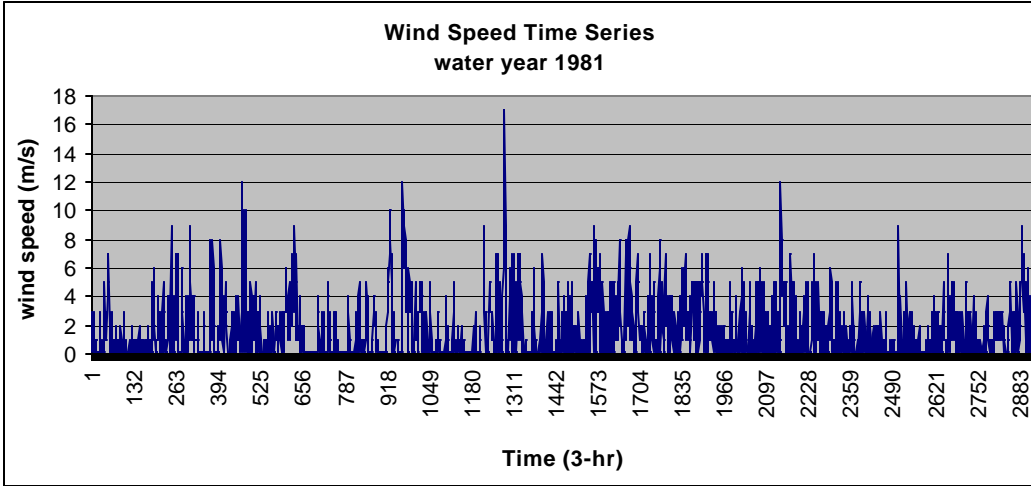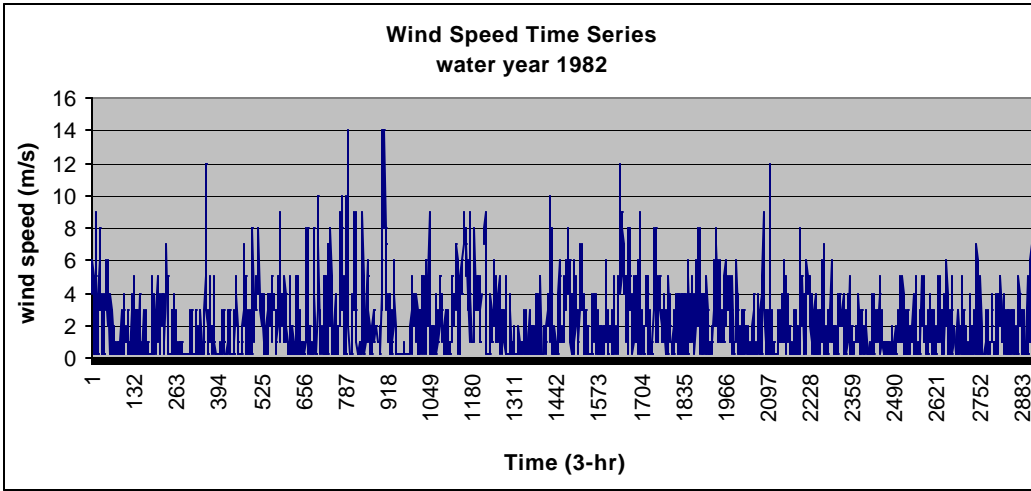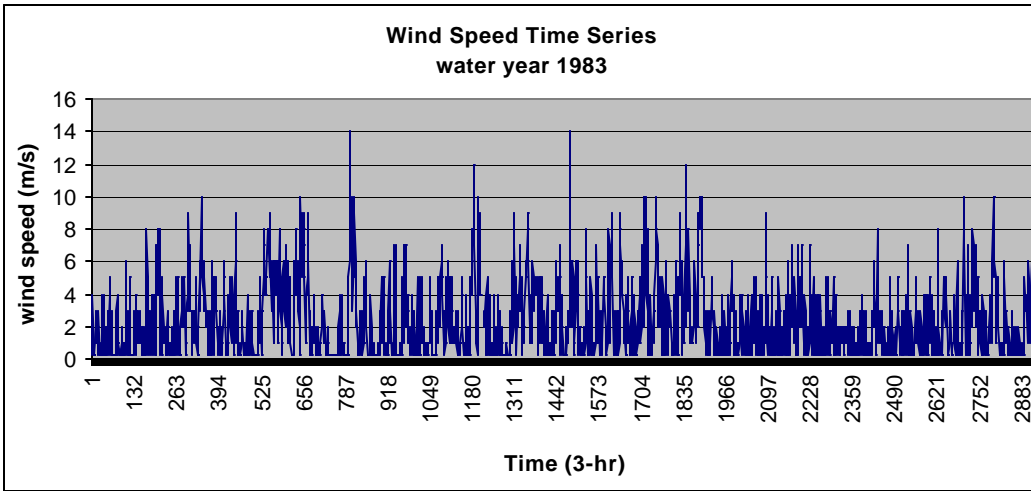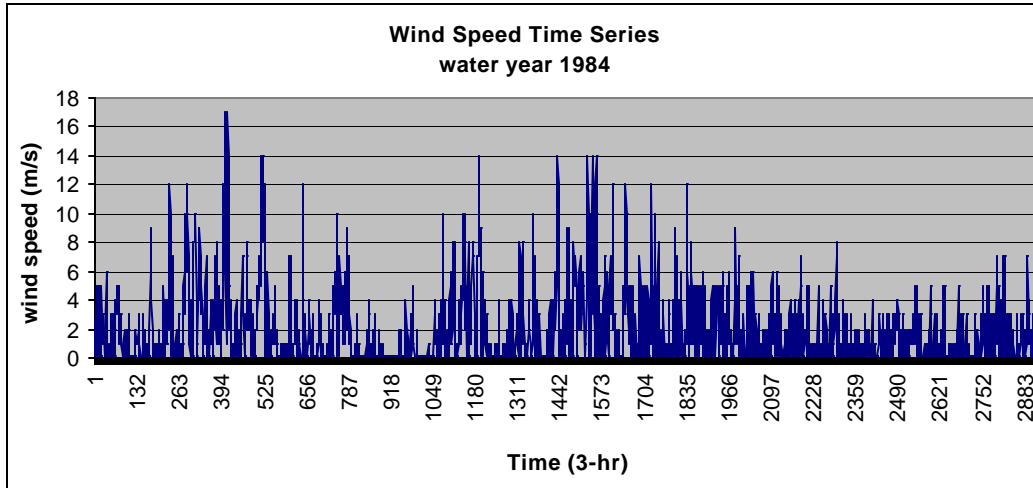
(d)
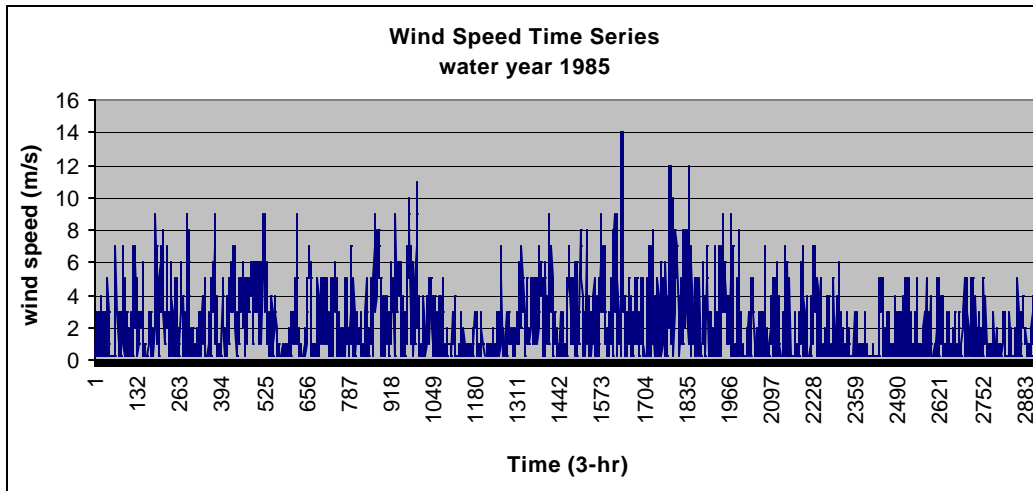
(e)
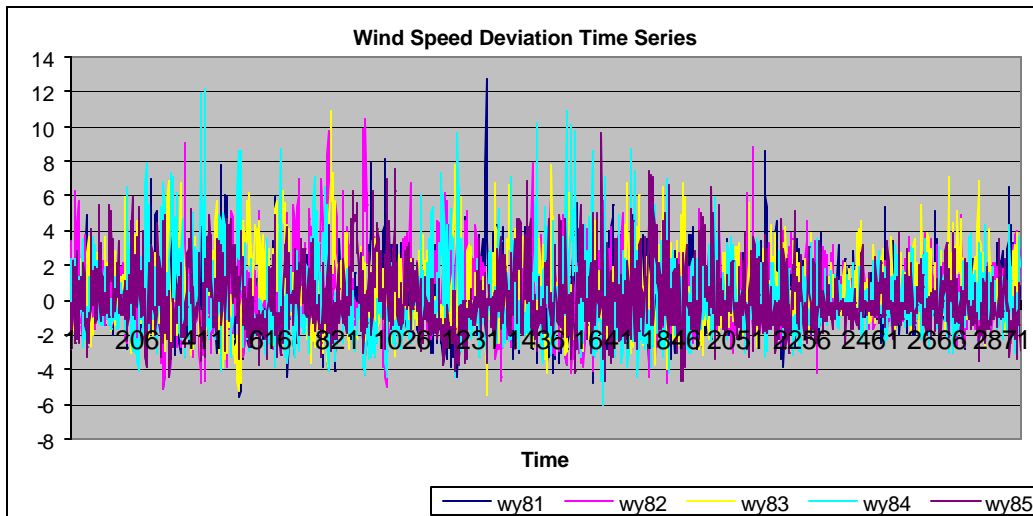
(f)

Figure 3.19 (a-e) Time series of wind speed for each water year. Figure 3.19(f) shows the deviation of the time series from the 5 -yr average

50

Relative Humidity. The relative humidity was assumed to be the equal to the value at

Tomsk for each point in the basin. (**Figure 3.21**)

Clear-Sky Shortwave Radiation. The clear-sky short-wave radiation was also assumed to

be the same as the measurement point throughout the basin. Actual radiation at each

simulation point is affected by cloud cover. (**Figure 3.22**)

3.5.2.2 Calculation of Evapotranspiration at Simulated Locations

All of the other inputs into the Penman Monteith Equation were calculated for

each simulation point through a series of physically-based formulas.

$$\Delta = \frac{2508.3}{(T_a + 237.3)^2} e^{\frac{17.3 \cdot T_a}{T_a + 237.3}} \tag{3-16}$$

where ? was in units of kPa.

$$\boldsymbol{l}_v = 2.50 - 2.36 \cdot 10^{-3} \cdot T_a \tag{3-17}$$

where ?$_v$ was in units of MJ/kg.

$$\boldsymbol{g} = \frac{c_a \cdot P}{0.622 \cdot \boldsymbol{l}_v} \tag{3-18}$$

where ? was in units of kPa/K.

$$e_a^{'} = 0.611 e^{\frac{17.3 \cdot T_a}{T_a + 237.3}} \tag{3-19}$$

where e$_a$` was in units of kPa.
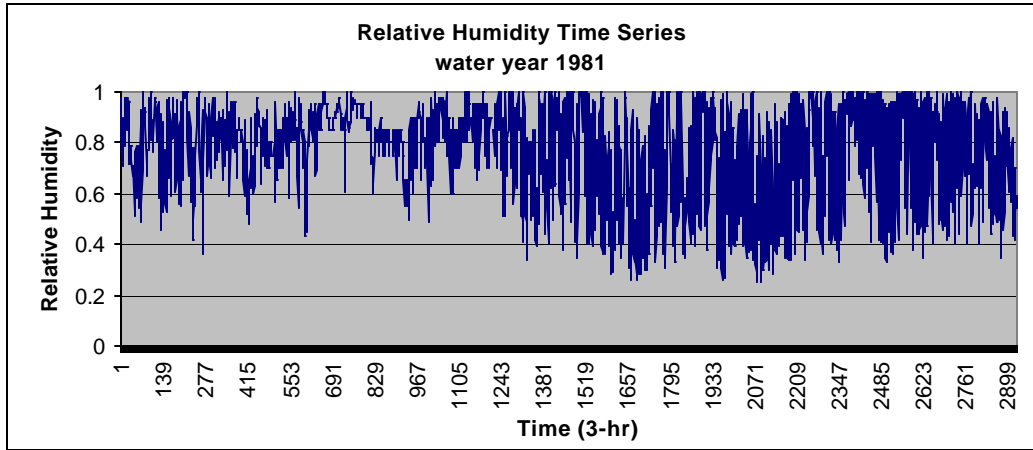
(a)
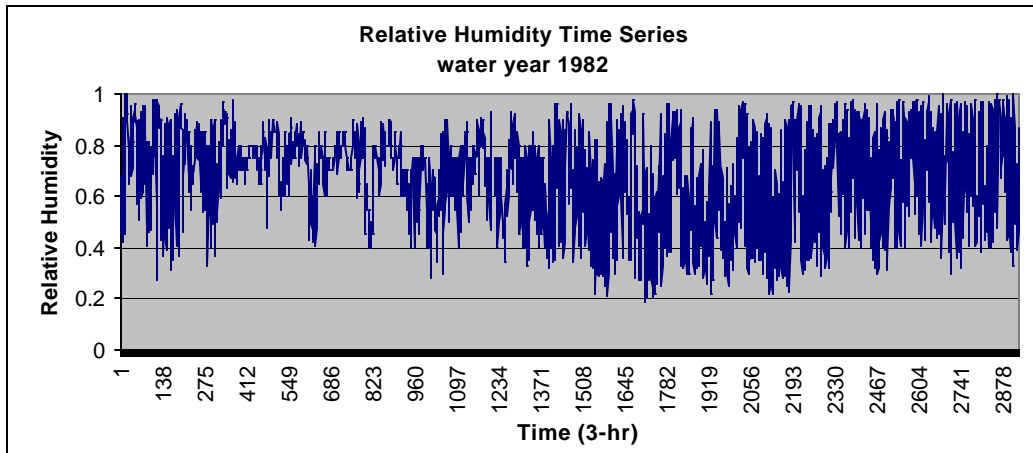
(b)
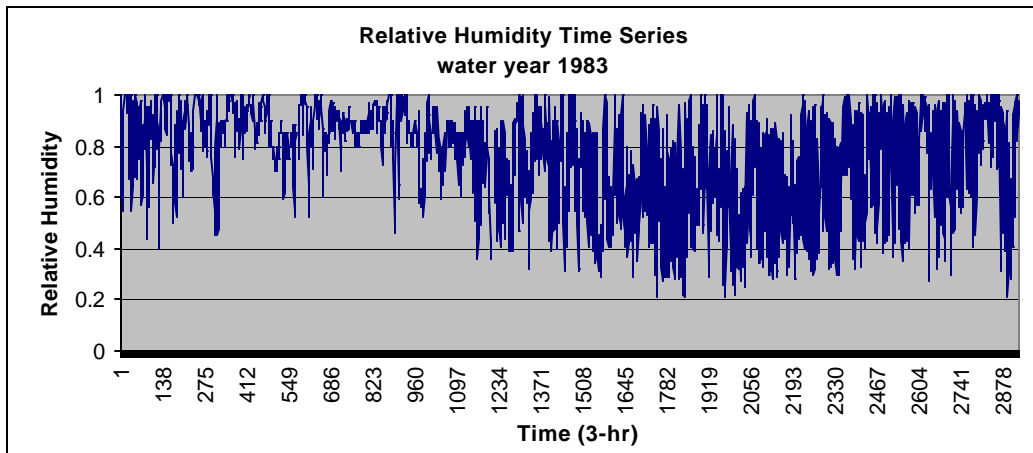
(c)
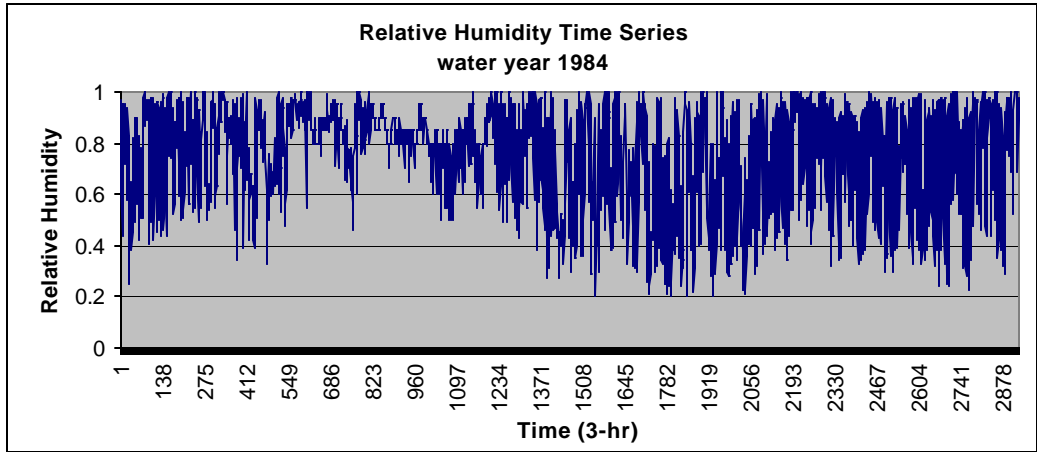
(d)
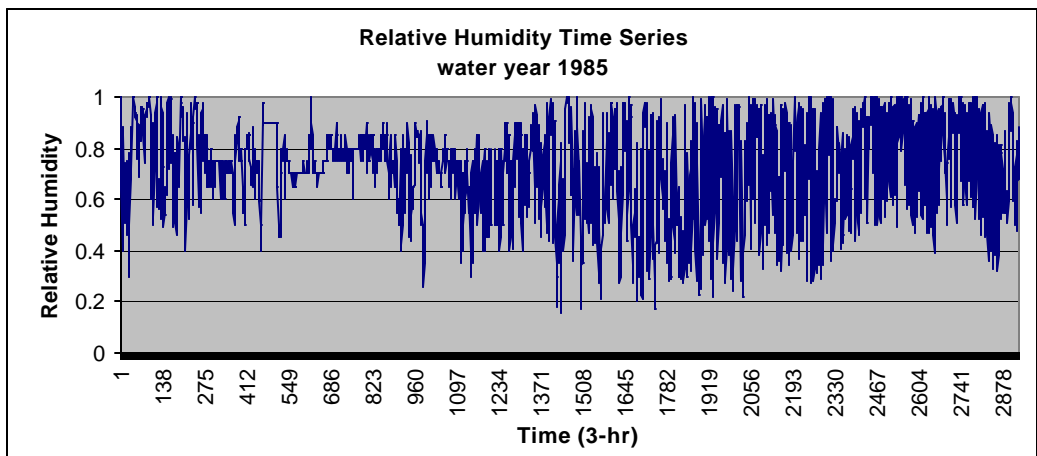
(e)
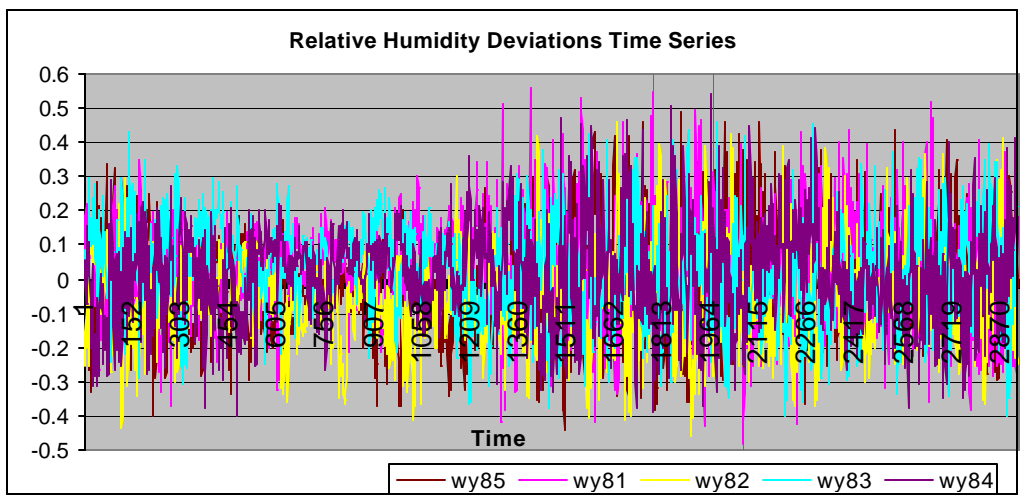
(f)

Figure 3.21 (a-e) time series of relative humidity for each of the water years. Figure 3.20(f) shows the deviation of the time series from the 5-yr average

(a)

(b)

(c)

54
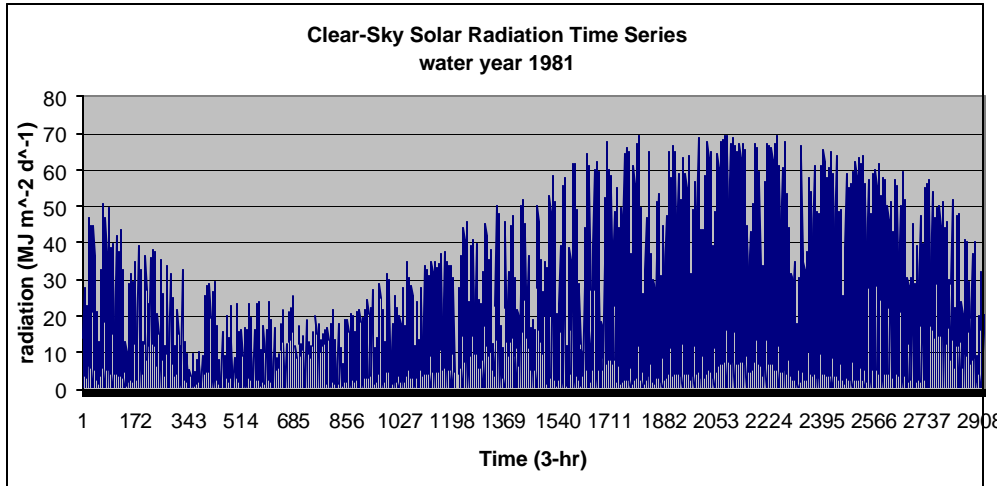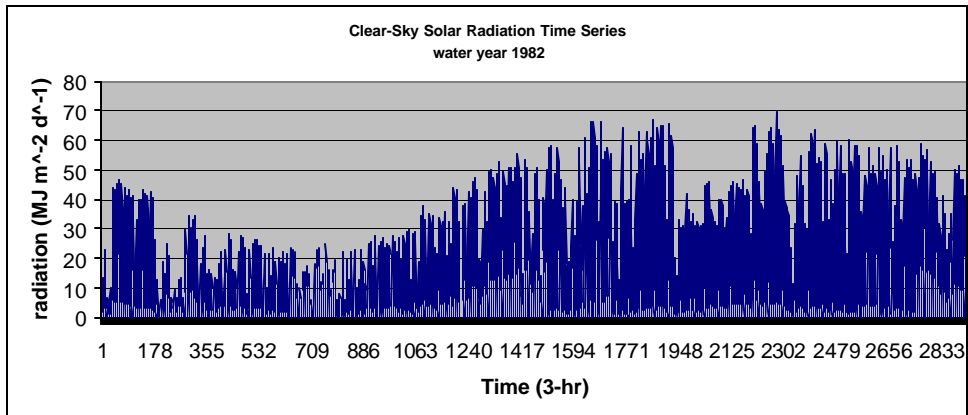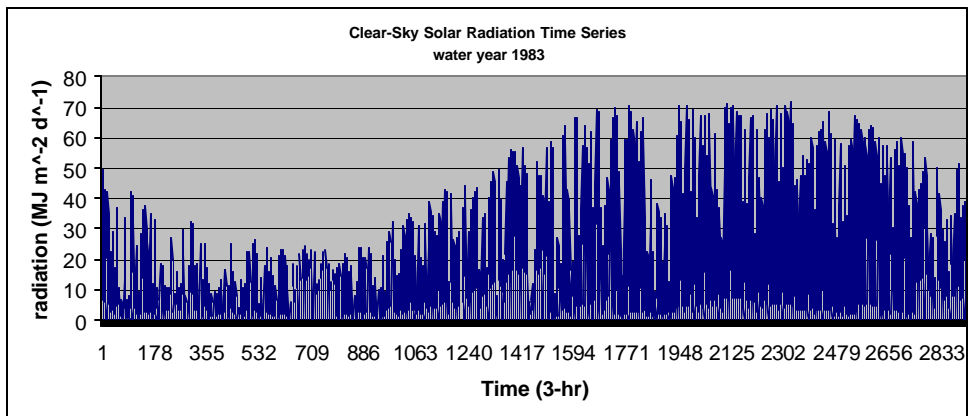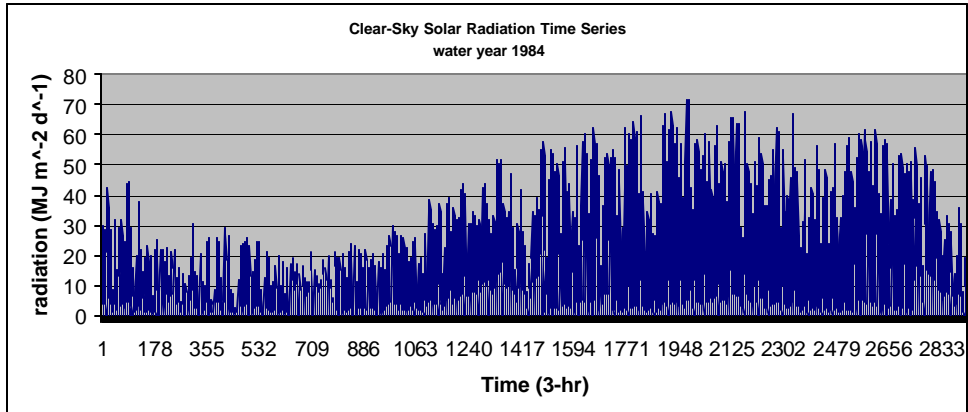
(d)
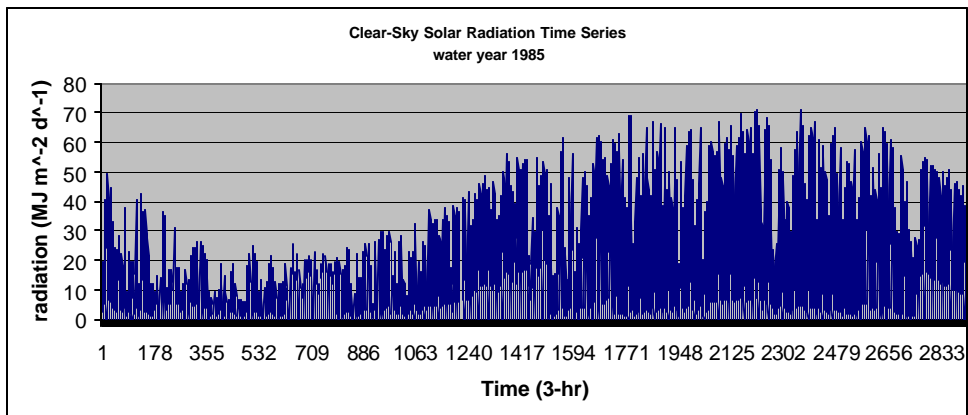
(e)
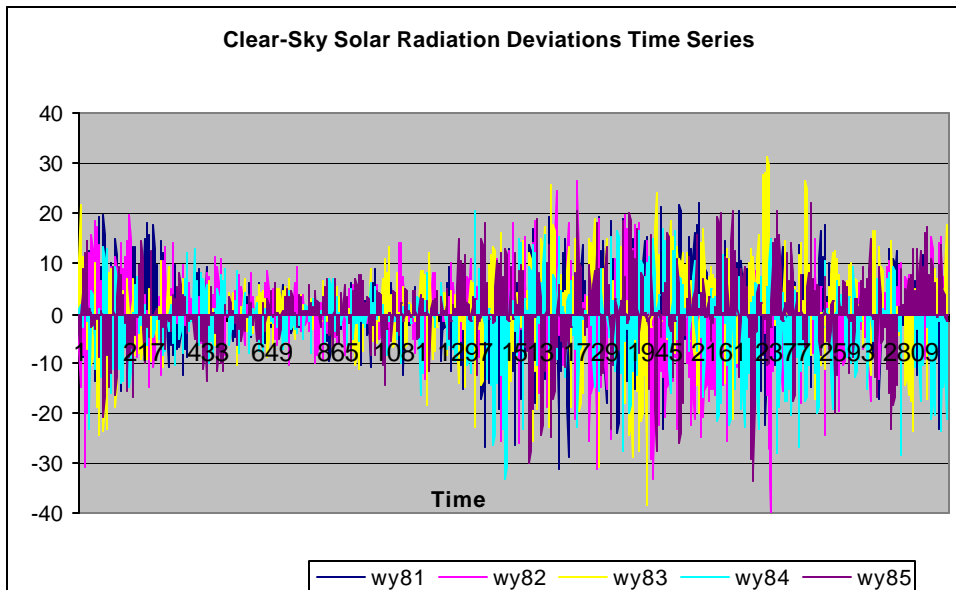
(f)

Figure 3.22 (a-e) time series of clear -sky solar radiation for each water year. Figure 3.21 (f) shows the deviation of the time series from the 5 -yr average.

55

$$r_a = \frac{352}{T_a + 273.2} \qquad \text{(3-20)}$$

where ρ_a was in units of kg/m^3

$$C_{at} = \frac{v_a}{6.25 \left[\ln \left(\frac{z_m - z_d}{z_0} \right) \right]^2} \qquad \text{(3-21)}$$

$$z_m = z_{veg} + 2 \qquad \text{(3-22)}$$

$$z_d = 0.7 \cdot z_{veg} \qquad \text{(3-23)}$$

$$z_0 = 0.1 \cdot z_{veg} \qquad \text{(3-24)}$$

where C_{at} was in units of m/s and ρ_a was in units of m/s, z_{veg} (m) is the height of the vegetation, z_d (m) is the zero-plane dispacement, z_m (m) is always assumed to be 2 m above the top of the vegetation, z_0 (m) and is the roughness height.

$$L = e_w \cdot e_{at} \cdot s \cdot (T_a + 273.2)^4 - e_w \cdot s \cdot (T_s + 273.2)^4 \qquad \text{(3-25)}$$

where ε_w is a constant with a value of 0.97, σ is the Stefan-Boltzman constant with a value of 4.90×10^{-9} MJ m^{-2} day^{-1} K^{-4}, and ε_{at} is the effective emissivity of the atmosphere calculated with the following equation

$$e_{at} = 1.72 \cdot \left(\frac{e_a}{T_a + 273.2} \right)^{\frac{1}{7}} \cdot \left(1 + 0.22 \cdot C^2 \right) \qquad \text{(3-26)}$$

where C is cloud cover ratio, and e_a (kPa) is the vapor pressure in the air given as

$$e_a = e_a' \cdot W_a \qquad \text{(3-27)}$$

The net shortwave radiation is given by the following equation

$$K = K_{in} \cdot (1 - a) \qquad \text{(3-28)}$$

where a is albedo, and K_{in} (MJ m^{-2} day^{-1}) is incoming shortwave radiation given by the following equation

$$K_{in} = [0.355 + 0.68(1 - C)]K_{cs} \qquad (3\text{-}29)$$

Finally, an evapotranspiration value was calculated for each time step at each point using equation 2-4. E was set to zero if the canopy conductance was zero. The total E for each simulation point was summed for each water year.

3.5.3 Sampling from Distributions using Random Number Generator

The Excel random number generator was used to generate random numbers from the assumed distributions. The random number was generated from the specified distribution by using the inverse of the distribution function. A test run of each distribution: gamma, beta, and uniform, was performed to ensure that each function worked. The parameters for each distribution were predefined. The parameters were used to create a probability density function (pdf) plot for a given range. 5000 numbers were generated using the random number generator. The numbers were grouped into histograms and the probability of each range was computed. This was plotted against the theoretical pdf. The mean, standard deviation, and parameters were calculated for each simulated pdf. These values were compared to the given values to ensure that the Excel random number generator was being applied properly for each distribution (**Figure 3.23**).
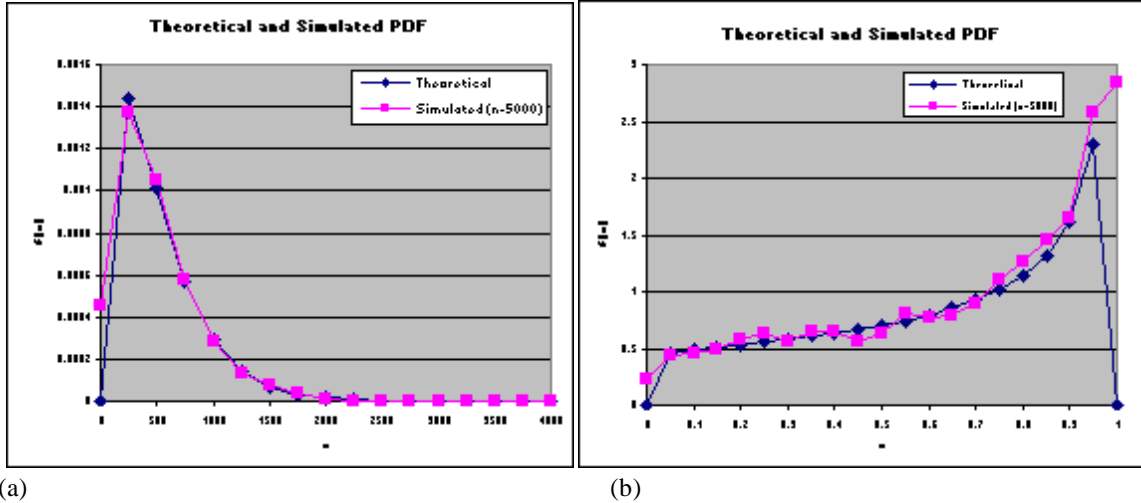
Figure 3.23: Comparison of theoretical distribution and simulated distributions from sampling of the (a) inverse gamma distribution and (b) inverse beta distribution. Number of simulated points was 5000

3.6 Hypothesis Test on Water Balance Closure

The water balance closure for each water year was calculated using equation 1-2. The variance of the water balance closure for each water year was calculated using equation 1-3.

A hypothesis test on the water balance closure as the mean was performed. In order to perform the hypothesis test the sample size had to be determined. Each component had different sample sizes so the composite sample size was unknown. An effective sample size was determined using the following equation from Haan (1977)

$$n_e = \frac{n}{\frac{(1+r_1)}{(1-r_1)} - 2r_1\frac{(1-r_1^n)}{n(1-r_1^2)}} \tag{3-30}$$

where n is the actual number of samples, and ρ_1 is the lag 1 autocorrelation coefficient.

Table 3.4 Effective sample size (n_e) determination for each water year

water year	Component	n	ρ_1	n_e
1981	streamflow	12	0.484897	4.253936
	ET	2920	0.743982	428.6734
	precip	12	0.543894	3.613203
1982	streamflow	12	0.464457	4.487959
	ET	2920	0.764908	388.9657
	precip	12	-0.2154	17.65269
1983	streamflow	12	0.432218	4.870323
	ET	2920	0.766933	385.1739
	precip	12	-0.11769	14.83767
1984	streamflow	12	0.220067	7.8461
	ET	2928	0.753107	412.3686
	precip	12	0.14451	9.130617
1985	streamflow	12	0.580497	3.240189
	ET	2920	0.752904	411.6272
	precip	12	0.580162	3.243513

Table 3.4 shows that the different data sources had very different effective sample sizes. The composite sample size for WBC is unknown. Lacking a good estimate of the true degrees of freedom for the problem, the z test (large-sample test) on the hypothesis of the mean was used. The z statistic is

$$z = \frac{\overline{x} - m}{s\sqrt{n}} \tag{3-31}$$

where $\overline{x}$ is the mean water balance closure for the water year, μ is the hypothesized population water balance closure, n is the effective sample size, and s is the standard deviation of the sample water balance closure.

The mean of the hypothesized water balance closure population was zero. The sample mean was the water balance closure calculated above. The standard deviation was the square root of the variance of the water balance closure calculated above. The null hypothesis is the water balance closure equal to zero, thus the alternative hypothesis is the water balance closure is not equal to zero.

$$H_0 : \mathbf{m} = 0$$
$$H_A : \mathbf{m} \neq 0$$

The two-sided test was performed to test if the water balance closure was zero. A one

sided test was not performed because it wasn't necessary to test if the WBC was less than

or greater then zero. The level of significance used was 10% and less.

4 Results

4.1 Introduction

In this chapter, analysis results are presented for the three terms in the water balance:

Precipitation (P), Streamflow (Q), and Evapotranspiration (E). The order of presentation

follows the order in which the methods were presented in Chapter 3. The chapter

concludes with the results of the hypothesis test on water balance closure.

4.2 Precipitation

Different decisions had certain effects on the results meaning the prediction estimation

model and the standard error of the estimates. The results were compared for datasets

with and without the outlier station 418.

4.2.1 Parameter Decisions

The semivariograms parameters mainly came from ArcGIS computations. Both

methods of optimizing the range and sill (NUMOPT and ArcGIS) gave similar values,

but the slight difference was noticed (**Tables 4.1-4.2**). For some of the years, the

semivariogram calculated within ArcGIS included a nugget, but the NUMOPT program

didn't have this option, so this could be the reason for some of the differences. A

semivariogram with less than 7 lags could not be modeled in ArcGIS, so there was no

way to compare the NUMOPT semivariograms to those of the other program. The least

amount of lags was modeled because the data seemed unrelated beyond the search radius

so modeling those extra lags would have been pointless.

Table 4.1: Semivariogram parameter decisions for analysis set w/o station 418

semivario-gram	lag size (m) & number of lags	range (m)	sill (mm^2)	Search nieghbor-hood	root mean square (Se)	mean error (mm)	average standard error	root mean square standardized	Se/Sy	Se/sill^0.5
wy81			Sy	157.16						
computed	100K, 7	309450	26400	10, 2	138.6	15.89	151.3	0.9412	0.882	0.890
		309450	26400	5, 2	138.3	14.72	151.6	0.9329	0.880	0.888
	100K, 13	272500	24250	10, 2	140.1	15.94	153.1	0.9278	0.891	0.900
		272500	24250	5, 2	140	14.11	153.3	0.9269	0.891	0.881
	100K, 15	286300	25230	10, 2	139.2	16.63	153.2	0.925	0.886	0.876
		286300	25230	5, 2	139.3	14.96	153.3	0.9252	0.886	0.877
computer	100K, 7	302190	27078	10, 2	138.2	16.27	154.8	0.9105	0.879	0.840
		302190	27078	5, 2	138.4	14.55	155	0.9114	0.881	0.841
	100K, 13	279720	25319	10, 2	139.8	16.14	154.9	0.9174	0.890	0.879
		279720	25319	5, 2	139.8	14.32	155	0.9165	0.890	0.879
	100K, 15	280460	25380	10, 2	139.8	16.16	154.9	0.9173	0.890	0.878
		280460	25380	5, 2	139.7	14.34	155.1	0.9164	0.889	0.877
wy82			Sy	180.19						
computed	100K, 8	439300	38020	10, 2	156.1	9.206	150.6	1.078	0.866	0.801
		439300	38020	5, 2	151.7	5.765	151.7	1.029	0.842	0.778
	100K, 13	323160	33360	10, 2	154.5	5.053	164.8	0.9598	0.857	0.846
		323160	33360	5, 2	151.4	3.507	165.2	0.9341	0.840	0.829
	100K, 15	307300	32270	10, 2	153.2	6.564	167.8	0.9416	0.850	0.853
		307300	32270	5, 2	152.5	5.921	168.1	0.9302	0.846	0.849
computer	100K, 8	330310	36339	10, 2	154	5.251	170.4	0.9282	0.855	0.808
		330310	36339	5, 2	151.3	3.759	170.8	0.9042	0.840	0.794
	100K, 13	296570	33571	10, 2	154.2	7.973	174.1	0.9071	0.856	0.842
		296570	33571	5, 2	153.8	6.752	174.4	0.9023	0.854	0.839
	100K, 15	294940	33450	10, 2	154.2	7.942	174.2	0.9066	0.856	0.843
		294940	33450	5, 2	153.8	6.716	174.4	0.9018	0.854	0.841

Table 4.1 continued

wy83		Sy	164.31							
computed	100K, 6	299140	30920	5, 2	couldn't get results, lag number must be > 7					
	100K, 13	251950	27770	5, 2	164.2	3.984	169.6	1.024	0.999	0.985
	100K, 15	231300	25910	5, 2	162.2	4.959	169.1	1.002	0.987	1.008
computer	100K, 7	194470	29162	5, 2	159.4	8.656	190.7	0.8534	0.970	0.933
	100K, 13	193450	27528	5, 2	159.4	8.638	185.6	0.8766	0.970	0.961
	100K, 15	213470	27460	5, 2	162.4	11.49	179.3	0.9296	0.988	0.980
wy84		Sy	172.34							
computed	100K, 6	466900	39610	5, 2	couldn't get results, lag number must be > 7					
	100K, 13	248000	27500	5, 2	155.4	7.45	169.7	0.9023	0.902	0.937
	100K, 15	213500	24000	5, 2	164.8	16.66	167.6	0.9515	0.956	1.064
computer	100K, 7	331860	35460	5, 2	150.6	13.25	168.4	0.8887	0.874	0.800
	100K, 13	279480	31000	5, 2	155	13.34	171.6	0.8923	0.899	0.880
	100K, 15	275110	30420	5, 2	155.2	13.15	171	0.8958	0.901	0.890
wy85		Sy	188.15							
computed	100K, 9	461600	39800	5, 2	165.9	13.83	151.2	1.122	0.882	0.832
	100K, 13	333000	36070	5, 2	165.3	15.13	169.6	0.9876	0.879	0.870
	100K, 15	282700	32480	5, 2	166.9	16.69	174.9	0.9661	0.887	0.926
computer	100K, 9	329200	37832	5, 2	165.3	15.07	174.5	0.9589	0.879	0.850
	100K, 13	320610	37208	5, 2	165.4	14.91	175.1	0.9548	0.879	0.857
	100K, 15	290320	36277	5, 2	166.8	16.82	182.8	0.9254	0.887	0.876
	100K, 7	317520	36989	5, 2	165.1	16.34	175.9	0.9515	0.877	0.858

Note: Highlighted regions was the set of paramters chosen to model the semivariogram to produce prediction maps

Table 4.2: Semivariogram parameter decisions for ananlysis set w/ station 418

Water year	Standard Deviation (Sy)	lag size (m) & number of lags	range (m)	sill (mm^2)	Search neighbor-hood	root mean square (Se)	mean error (mm)	average standard error	root mean square standardized	Se/Sy	Se/sill^0.5
1981	217.33	100K, 7	573240	53938	10, 2	220.1	-9.247	158.5	1.212	1.013	0.948
			573240	53938	5, 2	205.2	-13.6	160.1	1.138	0.944	0.884
		100K, 13	570470	55381	10, 2	220.1	-9.271	161	1.193	1.013	0.935
1982	227.1	100K, 8	644600	63763	10, 2	204.9	-5.205	162.2	1.103	0.902	0.811
			644600	63763	5, 2	187.7	-10.24	163.8	1.016	0.827	0.743
		100K, 13	613240	61073	10, 2	205	-4.328	162.8	1.098	0.903	0.830
			613240	61073	5, 2	187.7	-9.882	164.5	1.011	0.827	0.760
		100K, 15	607440	60553	10, 2	205	-4.227	162.9	1.097	0.903	0.833
			607440	60553	5, 2	187.4	-9.811	164.6	1.01	0.825	0.762
1983	207.69	100K, 7	538810	50264	5, 2	215.2	-11.89	159.6	1.242	1.036	0.960
		100K, 13	530490	49612	5, 2	215.1	-11.81	159.9	1.24	1.036	0.966
1984	212.84	100K, 7	587580	58416	5, 2	195.5	-3.287	164.5	1.095	0.919	0.809
		100K, 13	499320	50880	5, 2	195	2.317	17.1	1.073	0.916	0.864
		100K, 15	494760	50424	5, 2	195	-2.27	167.1	1.073	0.916	0.868
1985	281.39	100K, 7	696420	92097	5, 2	262.8	-24.17	189.1	1.163	0.934	0.866
		100K, 9	736200	94496	5, 2	263.5	-24.51	186.1	1.184	0.936	0.857
		100K, 13	821780	102680	5, 2	265.2	-25.18	183.3	1.208	0.942	0.828

Note: Highlighted regions was the set of paramters chosen to model the semivariogram to produce prediction maps

It wouldn't have made a difference which semivariograms parameters were used, NUMOPT or ArcGIS, since the values were so close for most of the years, but we chose to use the values with the smallest standard error ratio. The standard error ratio was the main factor in determining the best-fit model. The standard error-sill ratio was also a determining factor. These values were generally around 80%. These are acceptable values, but not excellent where preferred values are less than 50%; however the computed values were still less than 100%. The mean error was also a factor. The desired value for this factor was zero or as close to it as possible. Most of the years the error was a positive 15 mm. This was an acceptable value compared to the range of precipitation data, 150 to 800 mm. The positive value indicates that the model tends to overpredict precipitation relative to the data.

The radius of influence was small relative to the spread of the data. This wasn't a problem because we wanted the estimated precipitation in the basin only. The extra points were used to improve the prediction accuracy of the model. Only a small number of lags were used to illustrate this fact. After the range of the data, the values became independent so there was no need to model all of the data points. However the extra points overall gave more confidence in the prediction values.

The errors were accurately assessed through the semivariogram. This was shown in the standardized root mean square. This value should be as close to 1.0 as possible showing that the root mean square of the errors was close to or equal to the average standard error. This would mean the semivariogram is accurately assessing the variability in the data.

65

The search neighborhood used only included a small amount of points, mainly up to 5

gages (**Tables 4.3-4.4**).

Table 4.3: Search neighborhood determination for analysis set w/o station 418

Gages in search radius	water year 1981		water year 1982		water year 1983		water year 1984		water year 1985	
	RMS	Se/Sy	RMS	Se/Sy	RMS	Se/Sy	RMS	Se/Sy	RMS	Se/Sy
2	140.2	0.8921	152.2	0.8447	163.1	0.9926	155.2	0.9006	170.6	0.9067
3	152.8	0.9723	166.1	0.9218	157.8	0.9604	161.2	0.9354	177.9	0.9455
4	138	0.8781	155	0.8602	159.7	0.9719	152	0.8820	167.1	0.8881
5	138.4	0.8807	151.7	0.8419	159.4	0.9701	150.6	0.8739	165.9	0.8817
6	138.3	0.8800	153.3	0.8508			152.3	0.8837	169.6	0.9014
7	138.6	0.8819	151	0.8380			150.8	0.8750	167	0.8876
8	138.4	0.8807	152.3	0.8452			150.9	0.8756	169.1	0.8987
9	138.2	0.8794	154.8	0.8591			151.2	0.8773	172.3	0.9157
10			156.1	0.8663			151.3	0.8779	173.3	0.9211

Table 4.4: Search neighborhood determination for analysis set w/ station 418

Gages in search radius	water year 1981		water year 1982		water year 1983		water year 1984		water year 1985	
	RMS	Se/Sy	RMS	Se/Sy	RMS	Se/Sy	RMS	Se/Sy	RMS	Se/Sy
2	216	0.99388	207.2	0.91237	231	1.11223	215.4	1.01203	268.6	0.95455
3	220.2	1.01321	205.6	0.90533	226.5	1.09057	214.1	1.00592	272.3	0.9677
4	217.1	0.99894	201.6	0.88771	223.8	1.07757	207.8	0.97632	271	0.96308
5	205.2	0.94419	187.7	0.82651	215.1	1.03568	195.5	0.91853	262.8	0.93394
6	207.6	0.95523	194.3	0.85557	221	1.06409	199	0.93497	268.7	0.9549
7	214.3	0.98606	197.3	0.86878	224.7	1.0819	201.5	0.94672	279.4	0.99293
8	215	0.98928	198.3	0.87318	224.6	1.08142	205	0.96316		
9	219.4	1.00952	202.8	0.893						
10	220.1	1.01275								

Note: RMS is the root mean square of the error, Se is the standard error also called RMS and Sy
is the standard deviation. The highlighted values were the number of points selected for the
search neighborhood

Only a small number of gages was needed because the radius of influence was small (the

range), so there were not a lot of gages in the search radius. Even if the radius of

influence was large, with numerous points, the increased amount of points wouldn't relay

more important information needed to improve the model. The extra points added the

same information as the points already in the circle. The amount of points chosen was

based mainly on the standard error ratio. For water year 1983 the value was smaller for 7

gages in the search neighborhood, but the mean error and average error were much

higher, so we chose to stay with the slightly larger standard error ratio. The ratios were

approximately equal so it wouldn't have had an effect on the prediction model.

The validation showed poor prediction ability, but only 10 points were used to

validate so this is an indication of the small amount of points used for validation and not

the overall accuracy of the model. However the error plots did show that the model was

not biased. The spread of the errors showed no trend meaning they have no local biases.
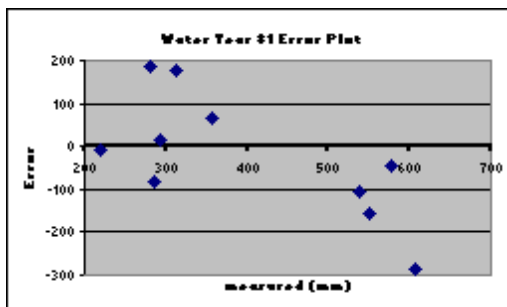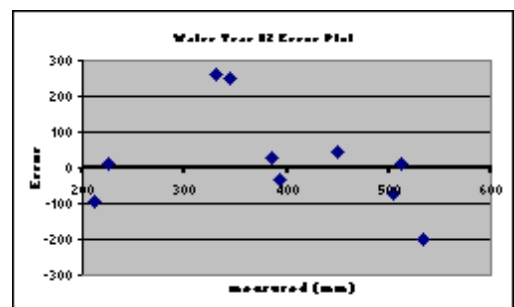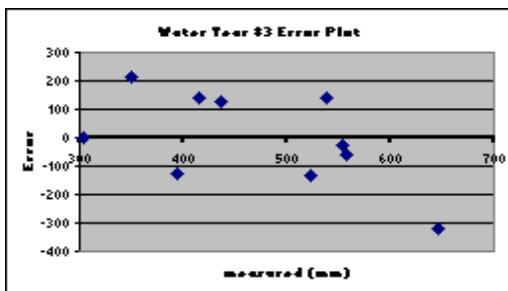
(**Figures 4.1-4.5**).

Figure 4.1

Figure 4.2

Figure 4.3
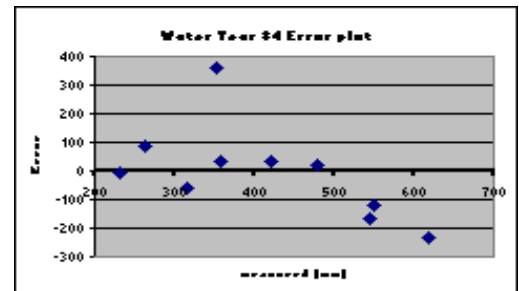
Figure 4.4
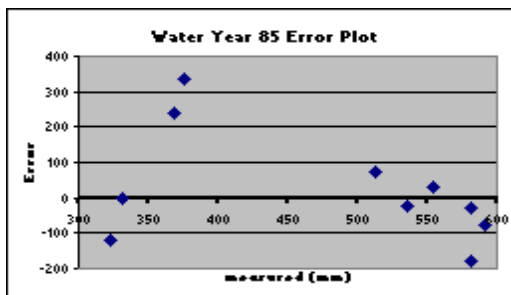
Figure 4.5

Figures 4.1-4.5 show measured precipitation values vs the error in the predicted values for the test gages

4.2.2 Discussion of Areal Coverage of Precipitation

The estimated average annual precipitation was consistent with average published ranges of 600 mm (Dutova et al., 1999) (**Figure 4.6**). As expected the mountainous regions had the largest values of precipitation. The estimated average basin precipitation for the analysis sets with ($\overline{P}_2$) and without ($\overline{P}$) station 418 is given in Table 4.5. Including station 418 slightly increased average basin precipitation.

Table 4.5: Estimated Average Basin Precipitation for each water year

	Wy 81	Wy 82	Wy 83	Wy 84	Wy 85
$\overline{P}$ (mm)	554.81	642.45	652.19	700.08	737.11
$\overline{P}_2$ (mm)	557.16	656.08	664.66	708.17	742.63

4.2.3 Discussion of Standard Error of Estimates

The mountain points (station 289 & station 418) were the source of much error in the model. Their quantity was much larger than many of the other points, but station 289 couldn't be discarded because it was one of two points in the basin. The argument for keeping station 418 (rather than discarding it as an outlier) was that it is one of very few measurements stations at higher elevations. These points introduced much error to the prediction model.

Kriging models tend to underestimate high measured values, while overestimating low measured values . This was the case with our models; it was much more dramatic with the analysis set including station 418. This affected the confidence in the model, but didn't have as much of an effect on the estimated values of precipitation in the basin. This is because the basin is small compared with the areal extent of the stations used. The width of the basin was typically smaller than the radius of influence.
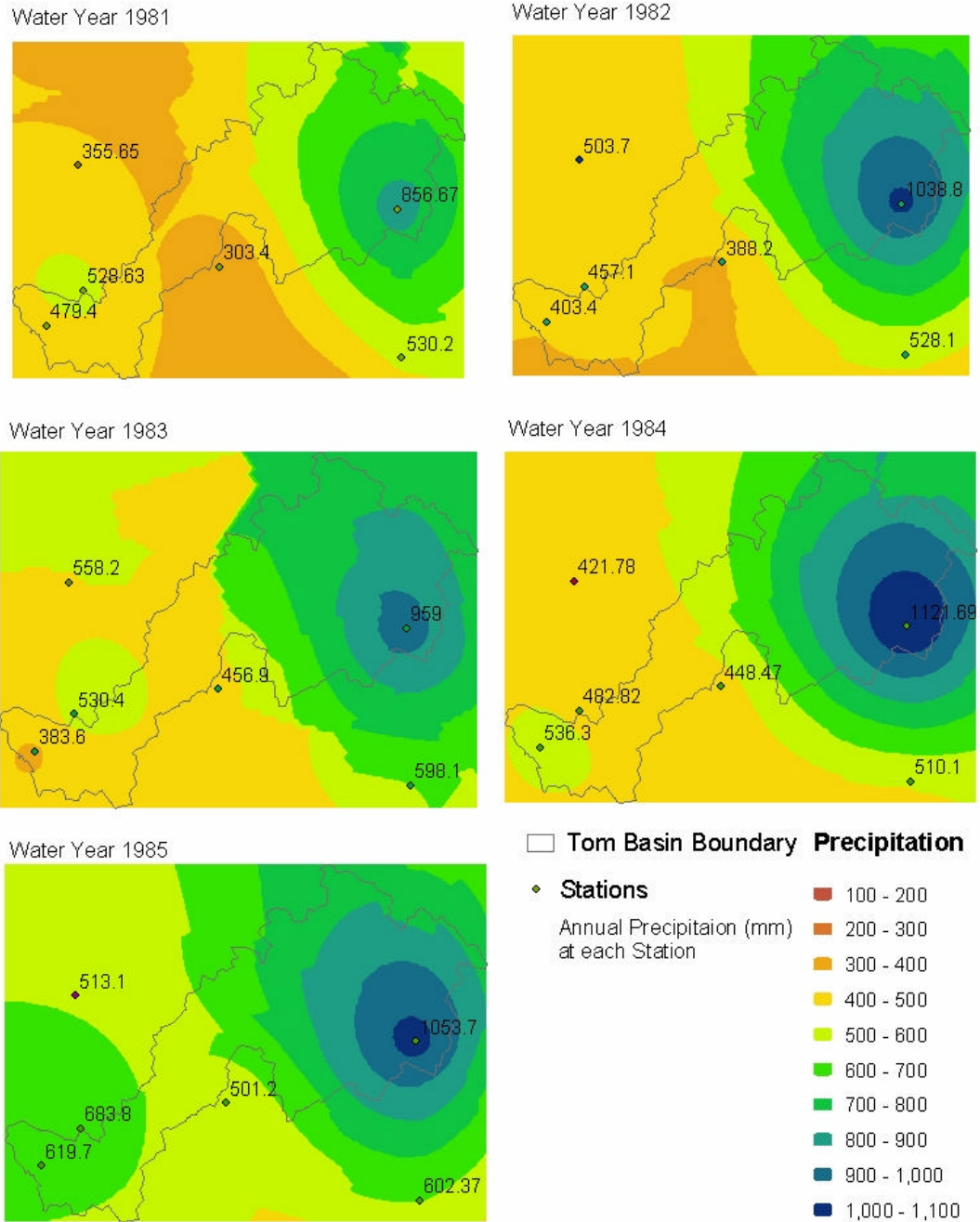
Figure 4.6: Precipitation prediction maps of the Tom Basin for each water year. Prediction maps were produced from Kriging interpolation method.

The kriged values at the station gages were very accurate; the standard error was small compared to the estimates in the rest of the basin. The higher amounts of error were in the mountainous regions in the northeastern corner of the basin (**Figure 4.7**).

4.2.4 Total Uncertainty in Annual Average Precipitation

The total uncertainty in the precipitation estimates for each water year computed using equation 3-4 is provided in Table 4.6.

Table 4.6: Variance of Estimated Precipitation for each Water Year

	Wy 81	Wy 82	Wy 83	Wy 84	Wy 85
$S^2(\overline{P})$ mm^2	271.0	541.6	271.2	541.9	541.8
$S^2(\overline{P})_2$ mm^2	537.2	537.2	537.3	537.2	1074

Table 4.7: Standard Deviation of Estimated Precipitation for each Water Year

	Wy81	Wy82	Wy83	Wy84	Wy85
$S(\overline{P})$ mm	16.46	23.27	16.47	23.28	23.28
$S(\overline{P})_2$ mm	23.18	23.18	23.18	23.18	32.78

The estimated variance of the estimated precipitation were approximately the same for water years 1981 and 1983 as well as 1982, 1984, and 1985. The sills for these two groups of years were approximately the same however the ranges of the semivariograms were not. The sills were the major influence in the calculation of the total error.

Station 418 had an impact on the total variance in the basin average of precipitation. The total variance of the estimated precipitation doubled in water year 1985; this was due to the large value of the sill. Again the values for water years 1981-1984 were similar where the sills of the semivariograms were similar in those years also. However in water year 1982 & 1984 the variance for the basin average precipitation was similar for both sets of analysis data, yet their sills were quite different.
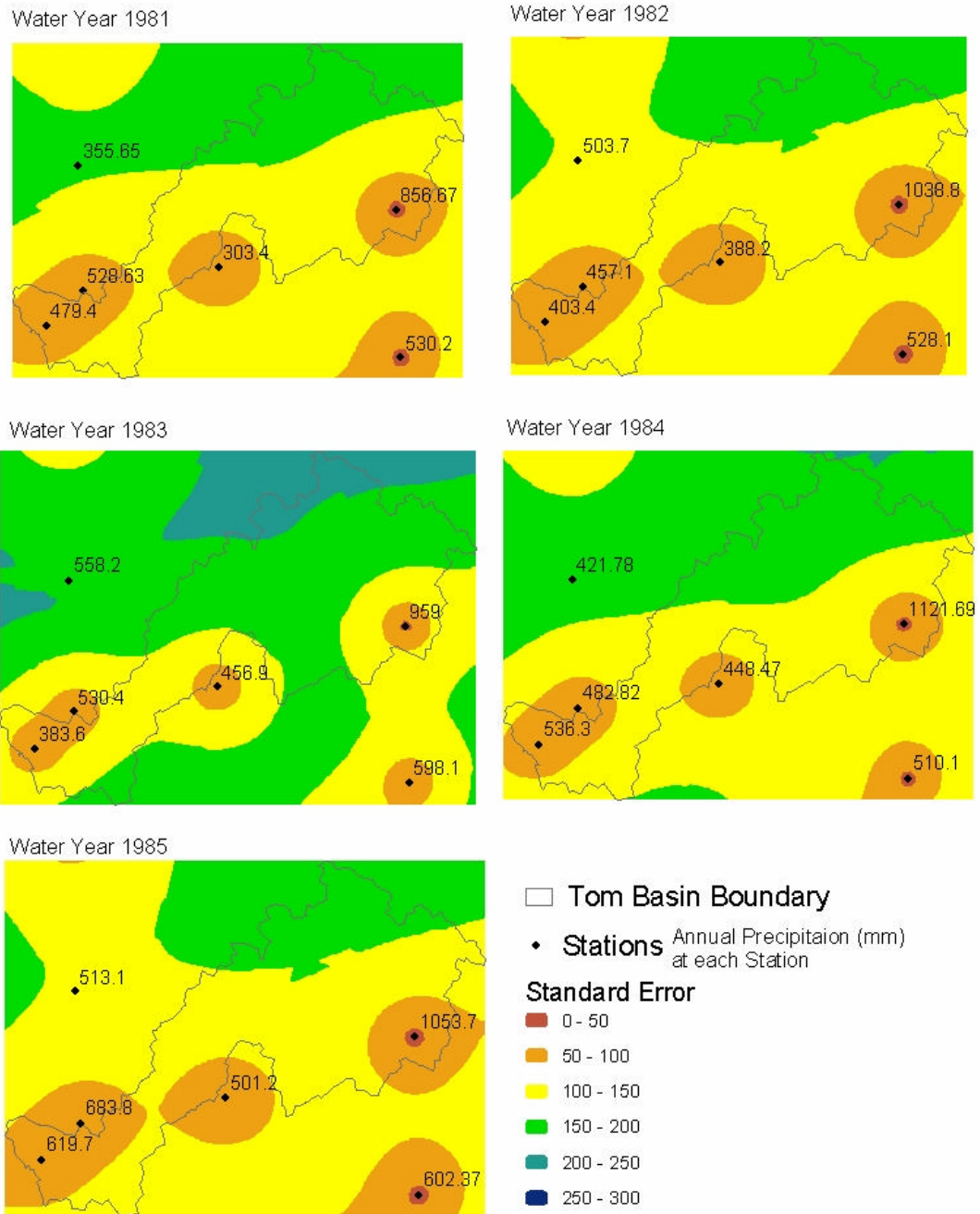
Figure 4.7: Maps of standard error (mm) of the estimated precipitation in the Tom Basin for each water year. Standard error maps were produced from the precipitation prediction maps.

4.3 Streamflow

The streamflow followed the same trend as precipitation; a gradual increase until water

year 1984, but then a decrease in water year 1985. The average annual streamflow,

variance, and standard deviation were as given in Table 4.8. The standard deviation of

annual streamflow was estimated at 5% of the total.

Table 4.8: Estimated Average Streamflow and the variance and standard deviation of the estimate for each Water Year

	Wy 81	Wy 82	Wy 83	Wy 84	Wy 85
$\overline{Q}$ (mm)	406.7	454.2	607.7	696.1	667.8
S($\overline{Q}$) (mm)	20.34	22.71	30.38	34.80	33.39
S^2($\overline{Q}$) (mm^2)	413.6	515.7	923.1	1211	1114

4.4 Overview of Evapotranspiration

Annual Evapotranspiration estimates showed a slight decrease until water year 1984, but

then an increase in water year 1985. Evapotranspiration estimates contained the most

uncertainty. This is consistent with our initial assumption. Evapotranspiration is a highly

variable process, and very hard to quantify accurately.

4.4.1 Spatial Distribution of Evapotranspiration and Results of Frequency Analysis

The values of simulated evapotranspiration ($\overline{E}$) were very close to the modeled values of

evapotranspiration from the NASA group ($\overline{E}_2$). The estimated average annual E is given

in Table 4.9. The E values were very similar throughout the study years.

Table 4.9: Estimated Average Evapotranspiration for each Water Year

	Wy 81	Wy 82	Wy 83	Wy 84	Wy 85
$\overline{E}$ (mm)	376.68	347.24	339.43	329.42	345.35
$\overline{E}_2$ (mm)	348.10	350.02	339.41	308.63	332.95

The total E values for the 1000 simulation points were grouped into histograms for each year. The frequency analysis showed a bimodal histogram (**Figure 4.8).** Although this bimdeality was not investigated in detail, it is probably due to the differences in vegetation type, as reflected by the conductance parameters in the Penman-Monteith equation.

4.4.2 Effects of Assumptions and Major Sources of Error

Two of the biggest assumptions made in this study were the elevation distribution and the vegetation coverage. From the available information, which were frequency analysis charts of elevation across the basin, the mean and standard deviation of elevation had to be estimated. This visible inspection introduced error in the assumed elevation distribution and its parameters.

The vegetation coverage was also estimated. The type of land cover and areal coverage in the basin had to be estimated based on existing information on the land types. Some of theses land types were not given in published information, so they had to be converted into the closest possible match in the published information. This uncertainty in the vegetation coverage introduced uncertainty in the E values.

The statistical distributions of the canopy characteristics were also estimated The spatial probability distribution and intraannual variation of canopy characteristics were specified based on physical reasoning and published values. Fortunately, for the
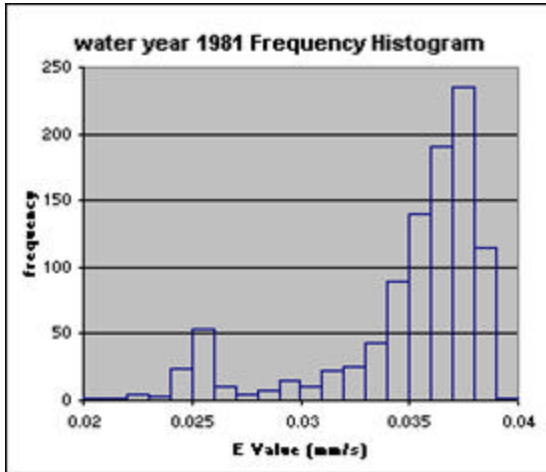
(a)
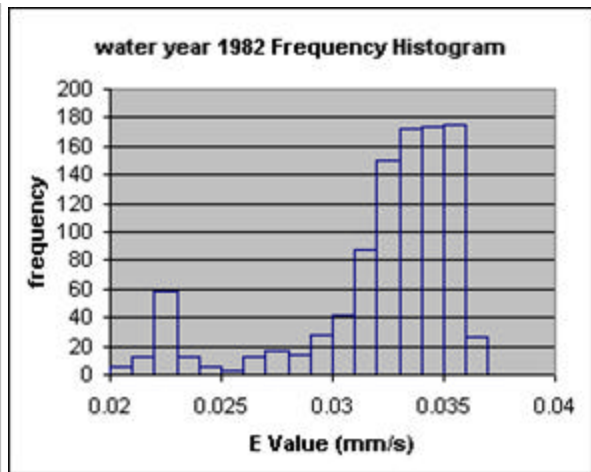
(b)
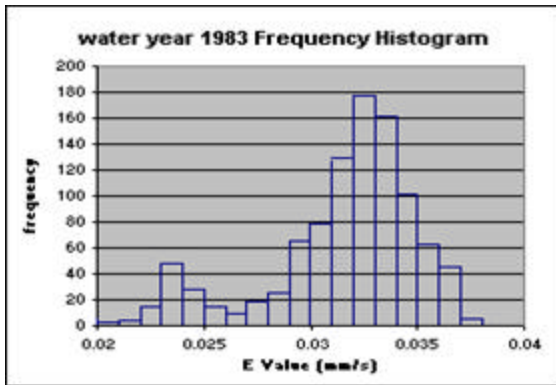
(c)
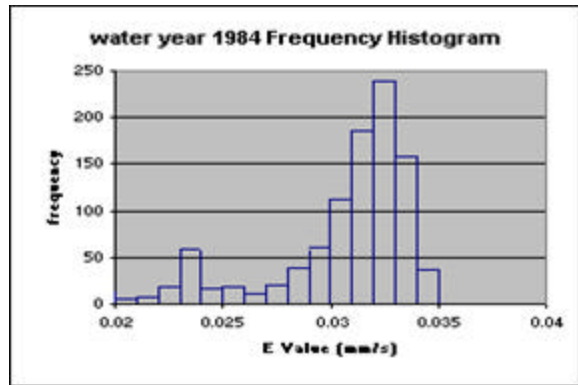
(d)
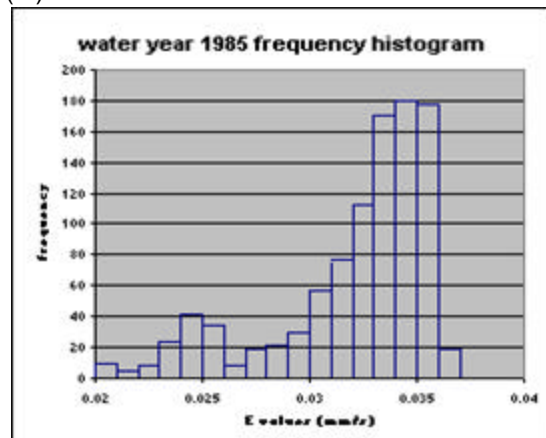
(e)

Figures 4.8(a-e): Histograms of annual E (mm/s) for each water year summed for all simulation points

winter months the canopy conductance was zero so these assumptions were less influential in the winter months, but for the rest of the year it is suspected that the assumptions had an effect on the resultant E values.

Another assumption made was that relative humidity was constant throughout the basin. This was done for simplifying purposes, based on an assumption that relative humidity is a general property of the air mass over a region and that it does not vary spatially at a given time. An argument can be made that this is not true, and that it may have been more appropriate to apply the same time-for-space substitution used for wind speed and cloud cover. A test of this assumption (and of the time-for-space substitutions) would require spatially distributed simultaneous observations, which were not available.

The soil moisture deficit model was created for this research. The beta factor was estimated based on visible inspection of soil type drainage profiles and an assumed soil type; this was a source of uncertainty in the model.

The number of simulation points chosen had an effect on the basin average evapotranspiration. The number was constrained to 1000 simulation points due to limited programming capabilities. The number used was sufficient for the method chosen to simulate E values. It can be shown that simulating 3000 or more points is more accurate for simulating the inputs to the E model, compared to the assumed theoretical distributions (Figures 4.9-4.12). The error becomes more consistent and decreases as more points are simulated. The effect of simulation points was only analyzed for vegetation, elevation, cloud cover, and wind speed because vegetation and elevation were the basis for most simulated inputs to the E model, and cloud cover and wind speed were independently simulated.
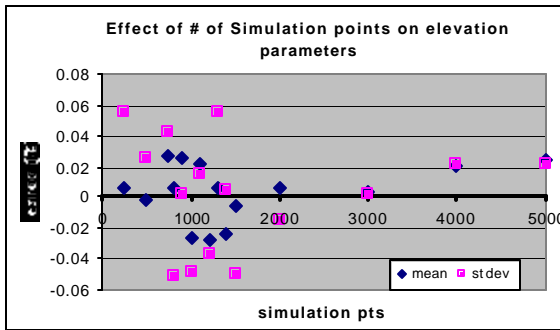
Figure 4.9 plot shows the number of simulation points affects the mean and standard deviation of the gamma distribution used to generate elevation
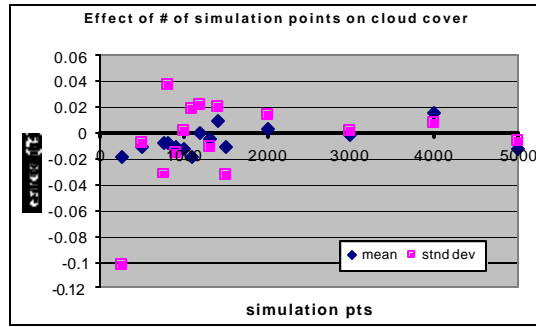
Figure 4.10 plot shows the number of simulation points affects the mean and standard deviation of the beta distribution used to generate cloud cover
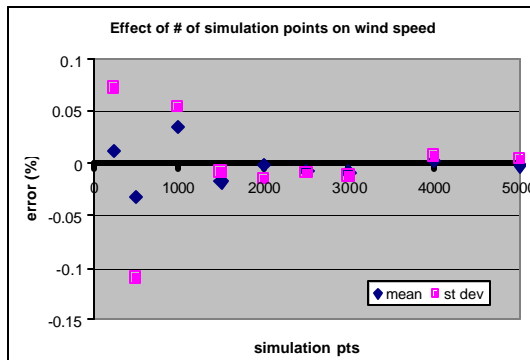
Figure 4.11 plot shows the number of simulation points affects the mean and standard deviation of the gamma distribution used to generate wind speed
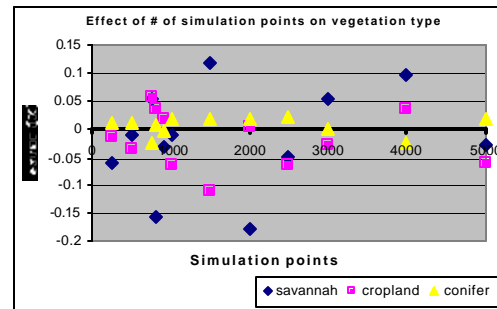
Figure 4.12 plot shows the number of simulation points affects the mean and standard deviation of the beta distribution used to generate cloud cover

The chosen 1000 simulation points was acceptable but 3000 or more points would have provided more confidence in the resultant basin average E and the standard deviation of the estimate (computational limitations are discussed in Chapter 5).

4.4.3 Total Uncertainty in Annual Average Evapotranspiraton

The total uncertainty in the simulated evapotranspiration values is shown in Table 4.10. E estimates contained the most uncertainty of the three water balance terms, as can be seen in the highest values of the variance of the estimated parameter.

Table 4.10: Standard deviation & variance of estimated E for each water year

	Wy 81	Wy 82	Wy 83	Wy 84	Wy 85
$S(\overline{E})$ (mm)	42.92	42.35	39.08	37.95	42.57
$S^2(\overline{E})$ (mm^2)	1842	1793	1527	1440	1813

4.5 Results of Hypothesis Test and Implications

4.5.1 Water Balance Closure and Variance of Water Balance Closure

The water balance closure and the variance of the closure are as given in Tables 4.11 and

4.12. The water balance closure is negatively biased for all water years. This is

consistent with our assumption that precipitation is underestimated thus negatively

biasing the water balance closure, although this does not constitute proof that P is

underestimated in the basin. Other explanations for a negative water balance closure

include:

- overestimated streamflow (Q)

- overestimated evapotranspiration (E)

- a decrease in storage during each of the five water years (this analysis assumed

  negligible change in storage over each water year).

Table 4.11: Water balance closure and variance of water balance closure for each water year for analysis set w/o station 418

	Wy 81	Wy 82	Wy 83	Wy 84	Wy 85
WBC (mm)	-228.6	-159.0	-294.9	-325.4	-276.0
S(WBC) mm	50.27	53.39	52.17	56.51	58.90
S^2(WBC) mm^2	2527	2851	2722	3193	3469
WBC as % of P	41	25	45	46	37

Table 4.12: Water balance closure and variance of water balance closure for each water year for analysis set w/ station 418

	Wy 81	Wy 82	Wy 83	Wy 84	Wy 85
WBC (mm)	-226.2	-145.3	-282.4	-317.3	-270.5
S(WBC) mm	52.85	53.35	54.66	56.47	63.26
S^2(WBC) mm^2	2793	2846	2988	3188	4002
WBC as % of P	41	22	42	45	36

4.5.2 Hypothesis Test

The null hypothesis that the water balance was actually zero was rejected for all tested

levels of significance for all water years for both analysis sets, based on the two-sided Z

test. For the set excluding station 418, the null hypotheses were rejected with rejection

probability of approximately 0.0% meaning there is an extremely small probability that

the water balance closures were actually zero. The set including station 418 had rejection

probabilities ranging from 0.0% to 0.36%. There was a slight increase in the probability

that the water balance closure is actually zero for the analysis set with station 418; this is

shown through the increased variance of the water balance closure. However the

probability is so small that it can be considered zero. Implications of the results are

further discussed in Chapter 5.

Table 4.13: Hypothesis Test Information for analysis w/o station 418

	wy81	wy82	wy83	wy84	wy85
Mean (mm)	-228.5934	-158.947	-294.899	-325.39	-276.022
Variance (mm^2)	2526.7907	2850.517	2721.521	3192.961	3469.091
standard deviation (mm)	50.267194	53.39023	52.1682	56.50629	58.89899
n_e	3.6132028	4.487959	4.870323	7.8461	3.240189
n	4	5	5	8	4
z	-9.095135	-6.65697	-12.6401	-16.2874	-9.37272
z(a = 0.1)	-1.281552	-1.28155	-1.28155	-1.28155	-1.28155
z(a = 0.05)	-1.644854	-1.64485	-1.64485	-1.64485	-1.64485
z(a = 0.025)	-1.959964	-1.95996	-1.95996	-1.95996	-1.95996
rejection probability	4.723E-20	1.4E-11	6.34E-37	6.06E-60	3.53E-21

Table 4.14: Hypothesis Test Information for analysis w/ station 418

	wy81	wy82	wy83	wy84	wy85
Mean (mm)	-226.2434	-145.317	-282.429	-317.3	-270.502
Variance (mm^2)	2792.9467	2846.164	2987.605	3188.31	4001.521
standard deviation (mm)	52.848337	53.34945	54.65899	56.46512	63.25757
n_e	3.6132028	4.487959	4.870323	7.8461	3.240189
n	4	5	5	8	4
z	-8.561989	-6.09078	-11.554	-15.8941	-8.5524
z(a = 0.1)	-1.281552	-1.28155	-1.28155	-1.28155	-1.28155
z(a = 0.05)	-1.644854	-1.64485	-1.64485	-1.64485	-1.64485
z(a = 0.025)	-1.959964	-1.95996	-1.95996	-1.95996	-1.95996
rejection probability	5.547E-18	0.003674	0.000321	9.47E-07	0.003359

Note: mean, standard deviation, and variance is the calculated water balance closure and its variance and standard deviation. Sample size, n, rounded value of effective sample size, n_e, was the sample size used for calculation of test statistic, z.

5 Conclusion

5.1 Summary of Results

This study has attempted to quantify the components of the annual water budget, precipitation (P), streamflow (Q), and evapotranspiration (E), and most importantly, the uncertainty in those components for the 57000-km^2 Tom River basin in Russian Siberia. The component terms and their corresponding uncertainty were calculated either from independent observational data or, in the case of E, using a physically-based model. The basin mean P was estimated by kriging analysis of available station observations; uncertainty in P was estimated as the standard error of the mean, derived from the kriging results. The annual mean Q was obtained from gage discharge measurements of the Tom at Tomsk, Russia; uncertainty in Q was computed based on published estimates of uncertainty in streamgage records. The basin mean and variance of E were computed from a statistical distribution based on Monte Carlo simulation of the Penman-Monteith (PM) model, driven by measured meteorological data at Tomsk, and accounting for physical variation in elevation and vegetation type as well as uncertain parameters of the PM model.

Uncertainty in the various terms arises from different sources, but each estimate of uncertainty can be expressed as a standard error, where "standard error" is the square root of the estimated error variance of the quantity (Weisstein, 2004). Annual average evapotranspiration contained the most uncertainty, with a standard error that ranged from 38 to 48 mm, whereas the standard errors of basin average streamflow and precipitation ranged from 20 to 35 mm and 16 to 23 mm, respectively.

Table 5.1: Summary of Results

	Wy 81	Wy 82	Wy 83	Wy 84	Wy 85
P_1 (mm)	554.8	642.5	652.2	700.1	737.1
P_2 (mm)	557.2	656.1	664.7	708.2	742.6
$S^2(P_1)$ (mm^2)	271	541.6	271.2	541.9	541.8
Error bar: $2S(P_1)$ (mm)	32.9	46.5	32.9	46.6	46.6
$S^2(P_2)$ (mm^2)	537.2	537.2	537.3	537.2	1074
Error bar: $2S(P_2)$ (mm)	46.4	46.4	46.4	46.4	65.6
Q (mm)	406.7	454.2	607.7	696.1	667.8
$S^2(Q)$ (mm^2)	413.6	515.7	923.1	1211.2	1114.8
Error bar: $2S(Q)$ (mm)	40.7	45.4	60.8	69.6	66.8
E (mm)	376.7	347.2	339.4	329.4	345.4
E_{PRMS} (mm)	348.1	350.0	339.4	308.6	333.0
$S^2(E)$ (mm^2)	1842	1793	1527	1440	1813
Error Bar: $2S(E)$ (mm)	85.8	84.7	78.2	75.9	85.1
WBC_1 (mm)	-228.6	-158.9	-294.9	-325.4	-276
$S^2(WBC_1)$ (mm^2)	2527	2851	2722	3193	3469
Error Bar: $2S(WBC_1)$ (mm)	100.5	106.8	104.3	113	117.8
WBC_2 (mm)	-226.2	-145.3	-282.4	-317.3	-270.5
$S^2(WBC_2)$ (mm^2)	2793	2846	2988	3188	4002
Error Bar: $2S(WBC_2)$ (mm)	105.7	106.7	109.3	112.9	126.5

Note: P_1 is average precipitation calculated from analysis set without station 418 and P_2 is average annual precipitation calculated from analysis set with station 418. E is simulation based average annual evapotranspiration and E_{PRMS} is weighted average evapotranspiration from NASA group

The uncertainty in the water balance was quantified by the variance of the annual Water Budget Closure, which is equal to the sum of the component variances. This calculation assumes that the errors in the components are independent, a reasonable assumption given that each of the components was computed from a different set of input data. Annual Water Budget Closure values were negatively biased ranging from -160 to -325 mm, and the standard error of Water Budget Closure ranged from approximately 50 to 60 mm. The hypothesis that the variance of the water balance closure was so large, that it in fact the WBC is zero was rejected at all levels of confidence (90% and above).

5.2 Implications and Contribution

Although the Water Budget Closure was negatively biased, this does not constitute

proof that precipitation is underestimated in the basin (as suspected at the outset of the

study). The negative water balance closure is an indication of water not being accounted

for in the analysis; however, the source of missing water is unknown. Possible

explanations for a negative Water Budget Closure can be identified by examining the

original equation,

$$WBC = P - Q - E - \Delta S \qquad\qquad (5\text{-}1)$$

If all terms of the water budget, including change in storage, were properly quantified,

WBC would equal 0. A negative WBC for a given water year indicates that either:

1. P is underestimated,

2. Q is overestimated,

3. E is overestimated, or

4. ΔS is overestimated,

or any combination of these. Each possibility is examined in turn, in the following.

Underestimated precipitation in the mountainous regions was originally presumed

to be a major factor in the water balance not closing. Additional evidence that basinwide

precipitation is underestimated is provided by computing runoff ratios for the five years.

The runoff ratio is defined as the ratio of discharge to precipitation, Q/P. A typical runoff

ratio for a high-latitude watershed is 0.25 (Dingman, 2002). The annual runoff ratios

computed for the Tomsk basin lie between 0.70 and 0.99; ratios greater than 0.70 are

unusual, and greater than 0.90 highly unlikely. In fact, the NASA modeling group has

found it necessary to augment the precipitation inputs in order to obtain physically-

realistic streamflows in their deterministic modeling. The gage data available do not support an orographic effect (increased precipitation at higher elevations). However, most of the gages are found at elevations below 500 m, and do not sample the higher elevations (see Figure 3.2); therefore a significant orographic trend was not detected in the data.

If the negative WBC is due to precipitation alone, then P for this basin would need to be underestimated by about 50 percent. This error is an order of magnitude greater than the error bars computed by kriging. That calls into question whether kriging is appropriate for estimating the true uncertainty in basin-average precipitation in this situation where a lack of quality data leads to model uncertainty.

A positive bias (overestimation) of stream discharge could result from overestimation of rating curves. Changes in streamflow could have occurred over the time period in question yet would not be reflected in the rating curve. The rating curve for the Tom River could have become outdated and not updated.

The Monte Carlo simulation method applied is what is considered the best available physically based evapotranspiration model. Many of the parameters required by the PM model are uncertain, and this analysis has attempted to identify the most reasonable estimates of those parameters, while also specifying possible ranges and quantifying uncertainty via assumed probability distributions of the unknown parameters. The uncertainty in the parameter distributions could have lead to the overestimation of E.

Information about water storage in the Siberian region was not known. Change in storage was assumed to be negligible or zero in computing the WBC; if in fact there was a decrease in storage, then this would explain the negative WBC. Storage decreases

could originate from decreases in surface water bodies (including reservoirs), soil moisture, groundwater, year-round mountain snowpack or glaciers. Data were not available to quantify these terms for the Tom River basin.

The use of the water balance must be done with caution due to the amount of uncertainty in the statement. Evapotranspiration contained the most uncertainty, and this level of uncertainty makes it difficult to assess the magnitude of the suspected bias in precipitation. The uncertainties in the components and the Water Balance Closure are an indication of the confidence that can be placed in statements about the water balance of the region under current or changing conditions.

For example, a large-scale water budget analysis such as this might be used to confirm predictions that large-scale warming in the Arctic will cause melting of permafrost, releasing fresh water from previously permanent storage. A negative WBC might seem to confirm that this is actually occurring; however, this conclusion would be premature without eliminating the possibility of bias in the components, especially P.

This research has demonstrated a new derived-distribution approach to estimating basin-average evapotranspiration and its uncertainty. These results can be compared to those obtained by a different, widely used approach: computing E as a residual, assuming negligible change in storage and dictating a perfectly-closed water balance:

$$E_{res} = P - Q \qquad (5\text{-}2)$$

Following Dingman, the error variance of E_{res} can be calculated as the sum of the variances in P and Q. This method was applied to the five study years to show how greatly E_{res} differs from E as computed by simulation. As shown in Table 5-2, such assumptions and such a method would have resulted in very small values of E for several

of the study years. It is interesting to note that the estimated error variance of E_{res} is generally less than that calculated from the derived distribution of E; it would be incorrect, however, to conclude on this basis that the E_{res} estimate is more accurate.

Table 5.2 Estimate of Evapotranspiration as a Water Balance Residual (E_{res}), compared to Simulation-based estimate (E_{sim})

	WY 81	WY 82	WY 83	WY 84	WY 85
E_{res} (mm)	148.1	188.3	44.53	4.03	69.33
S^2 (E_{res}) (mm^2)	684.6	1057	1194	1753	1657
Error Bar: 2S(E_{res}) (mm)	52.33	65.03	69.12	83.74	81.4
E_{sim} (mm)	376.7	347.2	339.4	329.4	345.4
S^2 (E_{sim}) (mm^2)	1842	1793	1527	1440	1812
Error Bar: 2S(E_{sim}) (mm)	85.84	84.70	78.16	75.89	85.15

The error variance, or error bar, quantifies precision, not accuracy, in the estimate. Neither the E nor the E_{res} estimate shown here is able to quantify the model error that results from neglecting change in storage in the former, and additionally forcing water balance closure in the latter approach.

5.3 Future Research

For watersheds like the Tom, it is difficult to predict future changes if the current state and fresh water fluxes are not well understood. This research demonstrates that unanswered questions remain about the supply and storage of water in the basin, and proposed new questions about the individual hydrologic components. Different ways to explore these issues include the investigation and quantification of the missing water in the water budget analysis and the investigation of the distribution of evapotranspiration values.

The negatively biased water balance closure for the basin needs to be investigated to determine whether it is due to underestimated precipitation in the mountains or a

significant decrease in storage in the basin. It is hoped that efforts to use remote sensing

to quantify snow water equivalent (SWE) in the mountains can address both the

hypothesized precipitation deficit and possible inter-annual changes in storage. The

methods developed in this project can be used to indicate if the SWE measurements

indeed decrease the gap.

Investigate the frequency distribution of evapotranspiration values. Our

frequency analysis showed a bimodal histogram; however, we were unable make

conclusions as to this occurrence. An increased number of simulation points would give

more confidence in the evapotranspiration statistics.

One extension of this research is to apply the methods of quantifying the

components and their uncertainty to the entire Ob basin to see how the results compare to

those achieved in this paper. Parts of the Ob basin are more densely gaged, with more

gages at higher elevations, so this might provide a more reliable precipitation estimate.

Future studies will investigate how the increased basin size and number of precipitation

gages translate to uncertainty in the estimates of the water budget components and

closure.

5.4 Lessons Learned

Technical skills were essential to completing this research. Learning the basics of a

newer version of ArcGIS was a massive task performed under personal tutelage. Once

the basics were learned, the geostatistical tool was explored to perform the necessary

tasks of this research. This tool is powerful with many different computational options;

those used in these tasks were only a portion of the many possibilities. The tool can be

misused if the internal procedures are not understood beforehand, which is a time

consuming task in itself. It was also important to understand the tool to verify the outputs.

Programming skills would have been a tremendous help in simulating the E values. A stand-alone program would have taken more time to develop, but would have been less time-consuming to run, and would have allowed a larger number of simulation points, as well as greater exploration of how different parameters contribute uncertainty in the simulated E.

References

ACSYS (1992). "Scientific Concept of the Arctic Climate System Study." WMO/TD No. 486, 89 pp.

Ahn, H. (1996). "Sensitivity for Correlated Input Variables and Propagated Errors in Evapotranspiration Estimates from a Humid Region." *Water Resources Research*, Vol 32(8): 2507-2516.

Andreassian, V., C. Perrin, and C. Michel (2004). "Impact of Imperfect Potential Evapotranspiration Knowledge on the Efficiency and Parameters of Watershed Models." *Journal of Hydrology*, Vol. 286: 19-35.

Anning, D. (2002). "Standard Errors of Annual Discharge & Change in Reservoir Content Data from Selected Stations in the Lower Colorado River Streamflow Gaging Network 1995-99."   Water Resources Investigation Paper, USGS.

Black, P. (1996). *Watershed Hydrology*, Ann Arbor Press, New York.

Brubaker, K. L., E. Josberger, A. T. C. Chang, and M. Jasinski, 2000. "Freshwater Fluxes of the Ob River Basin, Russia: Contribution of Snowpack in Complex Terrain." Research proposal submitted to the office of Earth Science National Aeronautics and Space Administration, subsequently supported by NASA as NAG 5-11600.

Deutsch, C. V. and A. G. Journel (1998). *GSLIB: Geostatistical Software Library and User's Guide*, Oxford University Press, New York.

Dingman, L. (2002). *Physical Hydrology*, Prentice Hall, Upper Saddle River, New Jersey.

Dingman, L. (1994). *Physical Hydrology*, Prentice Hall, Upper Saddle River, New Jersey.

Dingman, L., D. M. Seely-Reynolds, and R. C. Reynolds (1988). "Application of Kriging to Estimating Mean Annual Precipitation in a Region of Orographic Influence." *Water Resources Bulletin*, Vol 24(2): 329-339.

Drake, A. W. (1988). *Fundamentals of Applied Probability Theory, A McGraw Hill Classic Textbook Reissue*. McGraw Hill Inc., New York.

Dunne, T. and L. B. Leopold (2002). *Water in Environmental Planning*, W. H. Freeman and Co., New York.

Dutova, E.M., N. G. Nalivaiko, K. I. Kuzevanov, and J. G. Kopylova (1999). The

Chemical and Microbiological Composition of Urban Groundwater, Tomsk, Russia. In Chilton, J., Proc. XXVII Congress of International Association of Hydrogeologists, "Groundwater in the Urban Environment: Selected City Profiles" v. 2 Balkema, Rotterdam, 125-130.

ESRI (2001). *ArcGIS Geostatistical Analyst: Statistical Tools for Data Exploration, Modeling and Advanced Surface Generation*, ESRI White Paper.

Gagosian, R. B. (2003). "Abrupt climate change: should we be worried." http://www.whoi.edu/institutes/occi/currenttopics/climatechange_wef.html (accessed 8/2004)

Groisman, P., V. Koknaeva, T. Belokrylova, and A. Sanina. (1998). Former Soviet Union Monthly precipitation archive, 1891-1993. Boulder, CO: National Snow and Ice Date Center. Digital Media.

Hupet, F. and M. Vanclooster (2001). "Effect of the Sampling Frequency of Meteorological Variables on the Estimation of the Reference Evapotranspiration." *Journal of Hydrology*, Vol 243(3-4): 192-204.

Kondolf, G. M. and W. V. G Matthews (1991). "Unmeasured Residuals in Sediment Budgets – A Cautionary Note." *Water Resources Research*, Vol 27(9): 2483 2486.

Maidment, D. R. (1993). *Handbook of Hydrology*, McGraw Hill, Inc., New York.

McCuen, R. and B. M. Ayyub (2003). *Probability, Statistics, and Reliability for Scientist and Engineers*, Chapman and Hall, Florida

McCuen, R. (1998). *Hydrologic Analysis and Design*, Prentice Hall, New Jersey.

Mendenhall, W. and T. Sincich (1995). *Statistics for Engineering and the Sciences*, Prentice Hall, Upper Saddle River, New Jersey.

Milly, P. C. D and K. A. Dunne (2002). "Quantifying Errors in the Estimation of Basin Mean Precipitation." *Water Resources Research*, Vol 38(10): 13 pp.

Moges, S. A, Z. Katambara, and K. Bashar (2003). "Decision Support System for Estimation of Potential Evapotranspiration in Pagani Basin." *Physics and Chemistry of the Earth*, Vol 28(20-17): 927-934.

Montgomery, D. C. and G. C. Runger (1999). *Applied Statistics and Probability for Engineers & Scientists*, John Wiley and Sons, New York.

Moss, M. E. and E. J. Gilroy, 1980. "Cost-Effective Stream-Gaging Strategies for the Lower Colorado River Basin." United States Geological Survey Open File

Report, 80-1048.

NSIDC, Arctic Climate and Meteorology. Online at http://nsidc.org/arcticmet (accessed 8/2004)

Ormsby, T., E. Napoleon, R. Burke, C. Groessl, and L. Feaster (2001). *Getting to Know ArcGIS*, ESRI Press, California.

Saini, A. (2003). "Mapping Snow Cover in Siberia using GIS and Remote Sensing." MS Thesis, The University of Maryland, College Park, MD.

Sauer, V. B., and R. W. Meyer (1992). "Determination of Error in Individual Discharge Measurements." USGS, OFR-92-144.

Serreze, M. C., D. Bromwich, M. P. Clark, A. Etringer, T. Zhang, and R. Lammers (2002). "Large-Scale Hydroclimatology of the Terrestrial Arctic Drainage System." *Journal of Geophysical Research-Atmospheres*, Vol 108(D2): 28 pp.

Tsintikidis, D., K. P. Georgakakos, J. A. Sperfslage, D. Smith, and T. M. Carpenter (2002). "Precipitation Uncertainty and Raingage Network Design at Folsom Lake Watershed." *Journal of Hydrologic Engineering*, Vol 7(2):175-184.

UCAR/CSU, GLOBE program. Online at http://www.globe.gov (accessed 7/2004).

Vorosmarty, C.J., B. Fekete, and B.A. Tucker (1998). River Discharge Database, Version 1.1 (RivDIS v1.0 supplement). Available through the Institute for the Study of Earth, Oceans, and Space / University of New Hampshire, Durham NH (USA) at http://www.csrc.sr.unh.edu/hydro/.

Vorosmarty, C.J., B. Fekete, and B.A. Tucker (1996). River Discharge Database, Version 1.0 (RivDIS v1.0), Volumes 0 through 6. A contribution to IHP-V Theme 1. Technical Documents in Hydrology Series. UNESCO, Paris.

Wallace, J. and P. Hobbs (1977). *Atmospheric Science: an Introductory Survey*, Academic Press, London.

Weisstein, E.W. (2004). "Standard Error." From *MathWorld*--A Wolfram Web Resource. http://mathworld.wolfram.com/StandardError.html (accessed 11/2004).

Winter, T. C. (1981). "Uncertainties in Estimating the Water-Balance of Lakes." *Water Resources Bulletin*, Vol 17(1): 82-115.

Xu, Z. X and J. Y. Li, 2003. "Estimating Evapotranspiration Using Distributed Hydrologic Model." *Journal of Hydrologic Engineering*, Vol 8(2): 74-80.

"Oceans of the world." http://www.solcomhouse.com/oceans.htm (accessed 8/2004)